iScience

CellPress

Article

On the Immunological Consequences of Conventionally Fractionated Radiotherapy

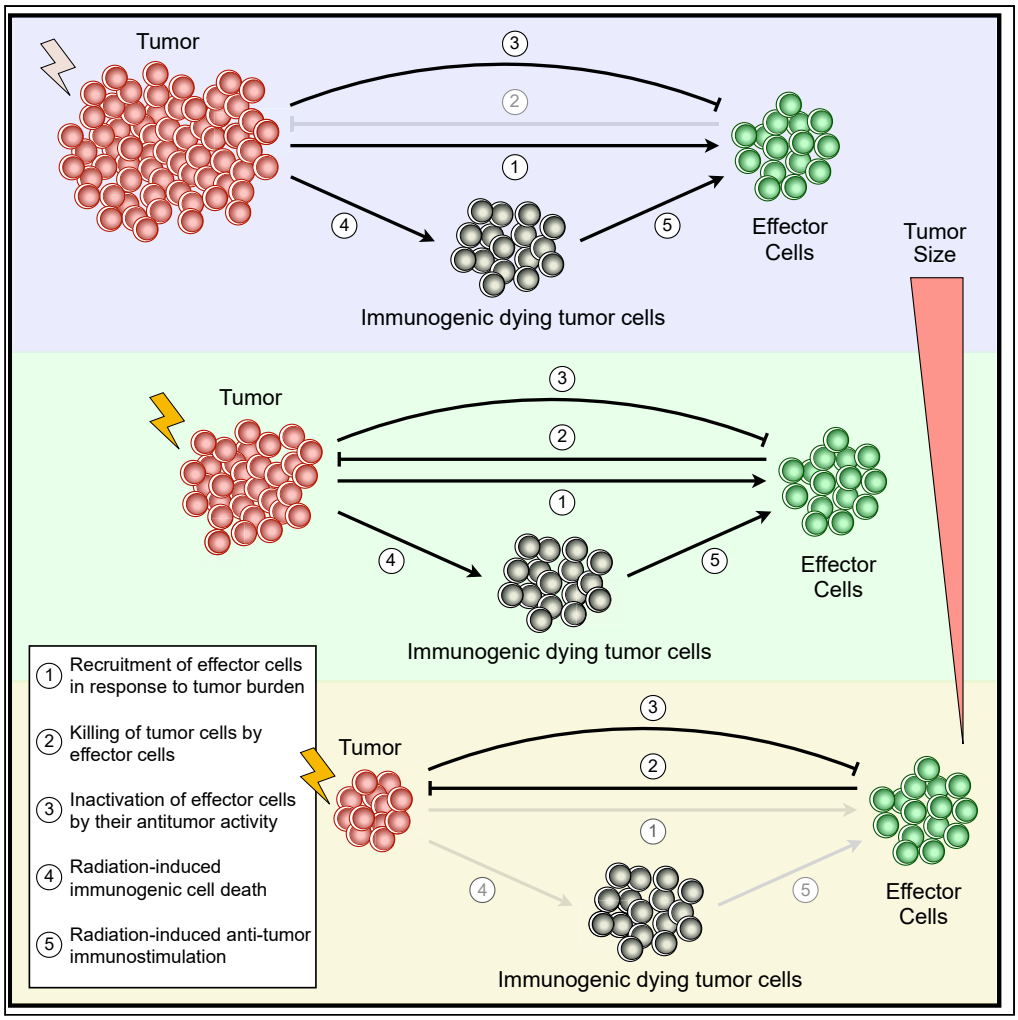

Juan Carlos L. Alfonso, Lito A. Papaxenopoulou, Pietro Mascheroni, Michael Meyer-Hermann, Haralampos Hatzikirou

mmh@theoretical-biology.de (M.M.-H.)
haralampos.hatzikirou@theoretical-biology.de (H.H.)

HIGHLIGHTS

Radiotherapy success depends on radiation-induced tumor-specific immune responses

Pre-treatment tumor size is not a consistent determinant of radiotherapy outcomes

Increase in treatment duration does not necessarily result in better tumor control

Tumor vascularity impacts antitumor efficacy of radiation-induced immune responses

Alfonso et al., iScience *23*, 100897
March 27, 2020
https://doi.org/10.1016/j.isci.2020.100897

iScience

CellPress

Article

On the Immunological Consequences of Conventionally Fractionated Radiotherapy

Juan Carlos L. Alfonso,[1] Lito A. Papaxenopoulou,[1] Pietro Mascheroni,[1] Michael Meyer-Hermann,[1,2,3,*] and Haralampos Hatzikirou[1,4,*]

SUMMARY

Emerging evidence demonstrates that radiotherapy induces immunogenic death on tumor cells that emit immunostimulating signals resulting in tumor-specific immune responses. However, the impact of tumor features and microenvironmental factors on the efficacy of radiation-induced immunity remains to be elucidated. Herein, we use a calibrated model of tumor-effector cell interactions to investigate the potential benefits and immunological consequences of radiotherapy. Simulations analysis suggests that radiotherapy success depends on the functional tumor vascularity extent and reveals that the pre-treatment tumor size is not a consistent determinant of treatment outcomes. The one-size-fits-all approach of conventionally fractionated radiotherapy is predicted to result in some over-treated patients. In addition, model simulations also suggest that an arbitrary increase in treatment duration does not necessarily result in better tumor control. This study highlights the potential benefits of tumor-immune ecosystem profiling during treatment planning to better harness the immunogenic potential of radiotherapy.

INTRODUCTION

Although a wide range of therapeutic strategies against cancer exists, radiotherapy (RT) remains one of the cornerstones in the treatment of localized solid tumors (Atun et al., 2015). Presently, over 50% of all cancer patients benefit from curative or palliative RT at some point during the course of their disease (Atun et al., 2015; Sharma et al., 2016). Advanced imaging techniques, coupled with improved planning methods and accurate delivery of prescribed doses, have made RT one of the most cost-effective form of non-surgical cancer treatment contributing to approximately 40% of cures (Sharma et al., 2016; Thariat et al., 2013). Despite the demonstrated efficacy of RT in many tumor types, several cancer patients still suffer from locoregional recurrence and development of distant metastasis, which is associated with intrinsic tumor cell radioresistance and intratumoral hypoxia extent resulting from functionally abnormal tumor vasculature (Begg et al., 2011; Horsman et al., 2012). Treatment failure is, in part, due to fractionation schemes routinely used in RT have been derived from empirical observations and average outcomes of large clinical trials, rather than obtained from a detailed knowledge of tumor-intrinsic features and microenvironmental factors (Barker et al., 2015; Schaue and McBride, 2015). Most importantly, radiation-induced changes in the immune system dynamics during and after treatment have not been considered in the planning process, thus limiting the potential benefits of RT.

RT has traditionally been perceived as an immunosuppressive modality (Formenti and Demaria, 2013; Lee et al., 2009; Roses et al., 2008). This is mainly attributable to the fact that tumor-infiltrating lymphocytes are regarded as radiosensitive cells (Liu et al., 2015), although the effects of dose-time fractionation schemes on the wide variety of tumor-infiltrating immune cell subsets remain unclear. The prevailing view of RT as immunosuppressive has been challenged by recent breakthroughs prompting a reevaluation of its potential as an adjunct to different anticancer immunotherapy strategies. Emerging evidence indicates that RT stimulates tumor-specific immune responses able to eliminate the residual cancer cells (Kaur and Asea, 2012; Roses et al., 2008). Radiation triggers immunogenic tumor cell death, leading to the release of tumor-associated antigens (TAAs) and damage-associated molecular patterns (DAMPs) that are subsequently presented by professional antigen-presenting cells (APCs) in the lymph nodes. This results in the priming and activation of tumor-specific effector T-cells, which then leave the lymphoid tissue, circulate in the bloodstream, and migrate into the tumor microenvironment to perform their cancer-killing function. The ability of RT to induce not only local but also systemic antitumor immunity has been reported (Formenti and Demaria, 2009, 2013). Immune-related antitumor effect of RT outside of the irradiated site has been reported for multiple cancer types, and it is known as the abscopal effect (Poleszczuk et al., 2016).

[1]Department of Systems Immunology and Braunschweig Integrated Centre of Systems Biology, Helmholtz Centre for Infection Research, Rebenring 56, 38106 Braunschweig, Germany

[2]Centre for Individualised Infection Medicine (CIIM), Feodor-Lynen-Straße 15, 30625 Hannover, Germany

[3]Institute of Biochemistry, Biotechnology and Bioinformatics, Technische Universität Braunschweig, Spielmannstraße 7, 38106 Braunschweig, Germany

[4]Lead Contact

*Correspondence: mmh@theoretical-biology.de (M.M.-H.), haralampos.hatzikirou@theoretical-biology.de (H.H.)

https://doi.org/10.1016/j.isci.2020.100897

Although the possibility of exploiting and rationally inducing efficient tumor-specific immune responses with RT is of high clinical interest, there are still many unanswered questions on the radiation synergy with antitumor immunity. In particular, it is poorly understood how the efficacy of RT-induced antitumor immune responses in achieving local control depends on tumor size at clinical presentation, duration of fractionation schedules, and direct effects of radiation on tumor-infiltrating cytotoxic lymphocytes during treatment. Increasing evidence suggests that tumor-associated vascularity is a determinant factor modulating the balance between tumor growth and dynamics of immune-mediated tumor clearance, thereby influencing tumor responses to RT (Hendry et al., 2016). Tumor-associated vasculature is not only critical to primary tumor progression and formation of distant metastases (Jain, 2005) but also influences radiosensitivity of tumor cells and infiltration of effector cells into the tumor parenchyma (Barendsen et al., 2001; Fridman et al., 2012; Rockwell et al., 2009). These vascular-mediated opposing effects on tumor-immune system dynamics are of particular importance, because they might determine RT outcomes. Thus, understanding the impact of tumor-immune ecosystem factors on the efficacy of radiation-induced antitumor immunity and tumor control probability is highly relevant to adapt or design patient-specific fractionation schemes to avoid under- or over-treating cancer patients, and inducing durable and effective antitumor immune responses, both locally and at potential distant metastatic sites.

Mathematical modeling of tumor growth, where some immune system components have been included, has long history (de Pillis et al., 2005; d'Onofrio, 2005; Eftimie et al., 2011; Hatzikirou et al., 2015; Kuznetsov and Knott, 2001; Matzavinos et al., 2004; Poleszczuk et al., 2016; Reppas et al., 2016; Robertson-Tessi et al., 2012; Wilkie, 2013). There are also several mathematical models of cancer treatment including RT, with the common overarching goals of expanding our knowledge on how tumor characteristics influence RT response and the development of novel optimized fractionation schedules (Alfonso et al., 2012; J. Alfonso et al., 2014; J. C. L. Alfonso et al., 2014; Enderling et al., 2006, 2010, 2019; López-Alfonso et al., 2019; Powathil et al., 2007; Rockne et al., 2009; Rockne and Frankel, 2017; Serre et al., 2016). However, models of tumor-immune system interactions to explore the influence of functional degree of tumor-associated vascularity and immunostimulatory effects of RT on tumor control have not been reported so far. Here, we extend a calibrated model of vascular tumor growth and associated tumor-specific adaptive immune responses to investigate the potential benefits and immunologic consequences of RT (Figure 1). The main novelty is that radiation-induced enhancement of antitumor immunity and the effect of radiation on both tumor and immune cells are considered. The proposed model is used to investigate the impact of tumor vascularization extent on (1) tumor growth, (2) recruitment of effector cells into the tumor bed, (3) efficacy of radiation-induced antitumor immunity, and (4) tumor response to RT. Moreover, the role of tumor size at time of RT and duration of fractionation schemes on radiation-immune system synergy and tumor control are explored. Although theoretical in nature, this *in silico* study provides motivation for prospective evaluation of the immunological consequences of RT in controlled *in vivo* experiments and clinical studies.

RESULTS

Tumor Vascularization Extent Impacts Antitumor Efficacy of Radiation-Induced Immune Responses

Tumor-associated vasculature is not only a pivotal determinant of tumor growth dynamic and radiosensitivity of cancer cells, but also influences the infiltration of effector cells into the tumor microenvironment. We simulated conventionally fractionated RT (50Gy in 25 daily fractions of 2Gy, 5 days per week) on tumors characterized by different extents of vascularization (B) and recruitment rates of effector cells in response to tumor burden (r). Simulations analysis suggested that there exists an intermediate range of tumor-associated vascularization degree resulting in tumor elimination after RT (Figure 2A). Figure 2B shows that radiation-induced immune responses might not be sufficient for complete tumor removal of poorly vascularized tumors with $B \leq 0.3$ and $r \leq 0.48$, whereas immune-mediated tumor removal after RT is observed for tumors with intermediate functional degrees of vascularization, i.e., $0.3 < B < 0.6$ (Figure 2C). These results are due to a combination of higher radiosensitivity, enhanced effector cell infiltration, and a more favorable antitumor immune contexture at the end of RT with increasing functional degree of tumor-associated vascularization. However, well-vascularized tumors with $B \geq 0.6$ escape because sufficient oxygen availability facilitates a faster tumor cell repopulation between RT fractions in comparison to treatment-induced tumor burden reduction (Figure 2D). In addition, tumor-immune ecosystems characterized by high rates of antitumor immune cell infiltration (r) enhance control probability of intermediate to poorly vascularized tumors (Figure 2A).

Extension of the analysis to different strengths of tumor-specific antitumor immune responses induced by radiation (η) and intrinsic proliferation rates of tumor cells λ_M confirms the critical role of tumor-associated

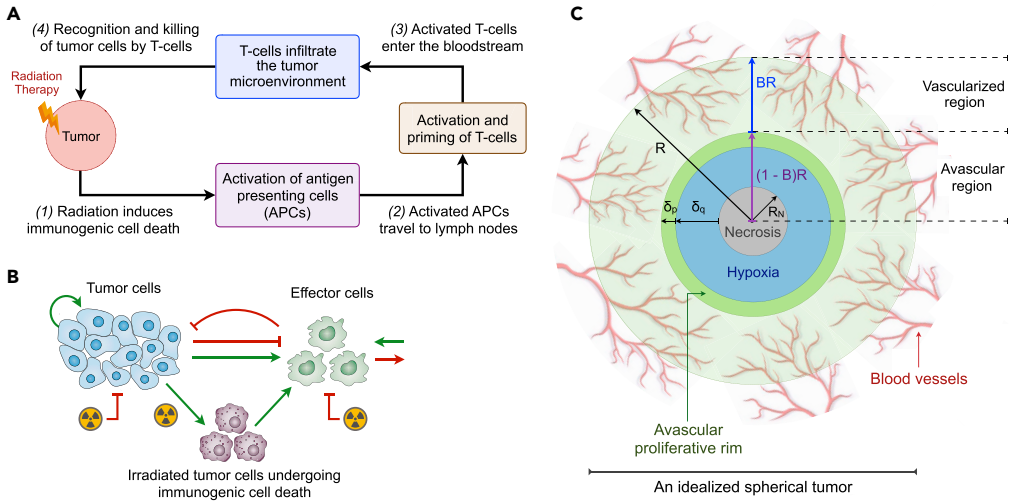

Figure 1. Model assumptions and schematic representation of system component interactions.

(A) Schematic view of RT-induced immune modulations. (1) Exposure to radiation induces the dying tumor cells to express significantly more tumor-associated antigens (TAAs) on their surface and release damage-associated molecular patterns (DAMPs). This promotes the activation of professional antigen presenting cells (APCs), which then (2) migrate to proximal lymph nodes (DLNs). Within the DLNs, T-cell exposure to activated APCs is mediated by direct contact, which results in priming and activation of T-cells. (3) Activated tumor-specific T-cells enter the bloodstream and infiltrate the tumor microenvironment, (4) recognizing cancer cells and performing tumor-specific killing.

(B) Schematic representation of the interactions between model components, where positive (green) and negative (red) feedbacks are represented.

(C) A cross sectional view of an idealized spherical tumor divided in an inner avascular region of radius $(1 - B)R$ and an outer vascular layer of thickness BR. The inner avascular tumor region is composed by an outer proliferative rim of thickness δ_p (dark green), an internal hypoxic layer of thickness δ_q (blue) and a central necrotic core (grey) of radius R_N.

vasculature on the antitumor efficacy of immune responses and RT outcomes (Figure S1 [Tumor vascularity and effector cell recruitment on response to radiotherapy]; related to Figure 2). Figure 2E shows that, as expected, increasing η results in better therapeutic success rates irrespective of λ_M values. In addition, the effectiveness of RT is limited by increasing inactivation rates of effector cells by their antitumor activity (d_1), decay rates of RT-induced tumor-specific immunity (θ), and intrinsic radiosensitivity of tumor cells (Figure S2 [Inactivation rate of effector cells on tumor response to radiotherapy and therapeutic success rate], Figure S3 [Decay of radiation-induced immunostimulation on tumor response to radiotherapy and therapeutic success rate], and Figure S4 [Intrinsic cancer cell radiosensitivity on tumor response to radiotherapy]; related to Figure 2). The aforementioned results suggest that the effectiveness of RT in eradicating tumors is determined by the direct lethal effect of radiation on cancer cells with the subsequent indirect effects of inducing tumor-specific immune responses.

Tumor Size Is Not a Determinant of Radiotherapy Outcomes

Intuitively, tumor size at time of RT would be expected to be a predictor of local failure. Indeed, large tumor size has been reported as a poor prognostic factor (Schaue and McBride, 2015; Sharma et al., 2016; Thariat et al., 2013). Simulations confirm that poor treatment outcomes of large tumors could be attributable to a limited burden reduction by radiotherapy. However, they also suggest that under certain conditions clinically detectable small tumors can escape treatment due to an insufficient radiation-induced antitumor immunity. Figure 3A shows that there exists an optimal (intermediate) tumor size before treatment (b.t.) for which the therapeutic success rate is higher from a certain strength of radiation-induced immune responses (η). Figures S5A and S5B [Intrinsic proliferation and surviving fraction of tumor cells on the therapeutic success rate; related to Figure 3] show how the pre-treatment size of tumors with different intrinsic proliferation rates (λ_M) and intrinsic radiosensitivity of tumor cells (i.e., surviving fraction of tumor cells at 2Gy) impacts the therapeutic success rate.

Figure 4A shows tumor responses for increasing pre-treatment tumor sizes, different infiltration rates of effector cells (r), and degrees of functional tumor-associated vascularity (B) to a conventionally fractionated RT protocol

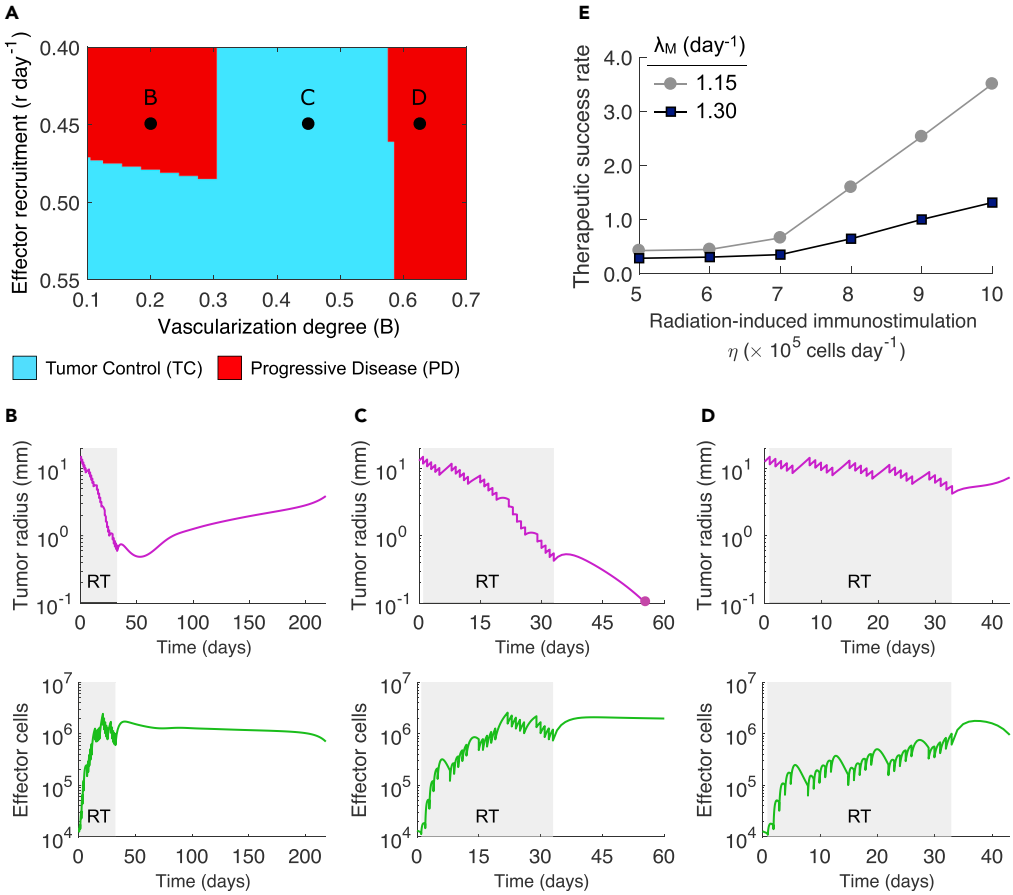

Figure 2. Effect of Functional Tumor Vascularization Extent and Strength of Radiation-Induced Immunity on Tumor Response to Radiotherapy

(A) Model-predicted tumor responses to RT depending on tumor-associated vascularity (B) and the recruitment rate of effector cells in response to tumor burden (r).

(B–D) Time evolution of tumor radius and effector cells during and after RT for parameter combinations marked in (A).

(E) Dependence of the therapeutic success rate with $0.40 \leq r \leq 0.55$ and $0.1 \leq B \leq 0.7$ on the strength of radiation-induced antitumor immune responses (η) and the intrinsic proliferation rate of tumor cells (λ_M). Radiation was delivered to a total dose of 50 Gy in 25 daily fractions at 2 Gy per day, 5 days per week. Tumor control (TC) (blue) and progressive disease (red) refer to tumor eradication and escape after treatment, respectively. Model simulations were performed with $\eta = 8.0 \times 10^5$ cells day^{-1}, $\lambda_M = 1.15$ day^{-1}, and a tumor size at time of RT equal to $R = 15$ mm, unless indicated otherwise.

The remaining parameter values were as in Table S1 [Parameter values considered in model simulations].

(50 Gy in 25 fractions of 2 Gy, 5 days per week). Simulations suggest that there is a close relationship between the functional degree of tumor-associated vascularization (B) and pre-treatment tumor size in determining RT outcomes. Long pre-treatment monitoring periods of tumor size are beneficial for poorly vascularized tumors ($B < 0.3$). This waiting time enhances vascular-mediated infiltration of effector cells, radiosensitivity of hypoxic tumor cells and induction of immunogenic cell death. However, this monitoring strategy before treatment is consistently detrimental on well-vascularized tumors ($B > 0.55$) due to the ability of cancer cells to proliferate faster under adequate oxygenation/perfusion conditions. Interestingly, intermediate-vascularized tumors ($0.3 \leq B \leq 0.55$) are more responsive to RT at an optimal tumor size at the time of treatment.

Simulations also reveal that there exists an optimal number of effector cells present in the tumor microenvironment after treatment (a.t.) at a certain pre-treatment tumor size (Figure 4B). This phenomenon is observed despite a consistent increase in radiation-induced recruitment of effector cells, and therefore systemic activation of antitumor immunity, with larger tumor sizes (Figure 4C). The size of tumors treated with RT, at which higher amount of effector cells a.t. is observed, depends on a delicate balance between radiation-induced level of immunogenic death, tumor burden reduction by RT, and development

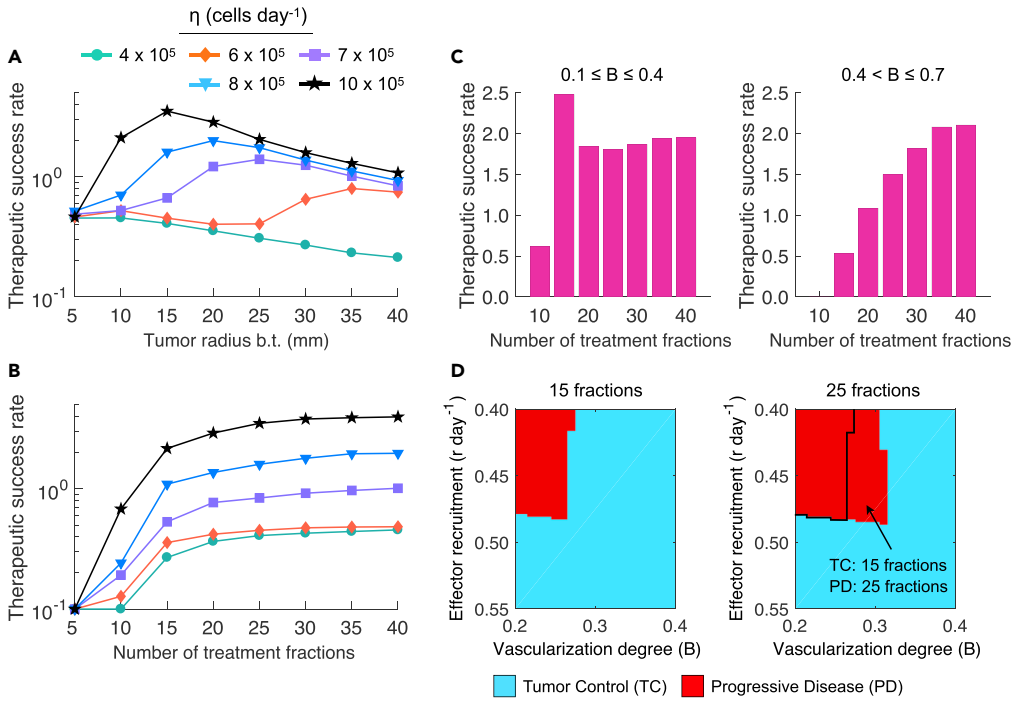

Figure 3. Effect of Tumor Size at Time of RT and Treatment Duration on the Therapeutic Success Rate

(A and B) Dependence of the therapeutic success rate with recruitment rate of effector cells in response to tumor burden $0.40 \leq r \leq 0.55$ and the functional degree of tumor-associated vascularity $0.1 \leq B \leq 0.7$ on tumor radius before treatment (b.t.) and the number of treatment fractions for increasing strengths of tumor-specific immunity induced by radiation (η).

(C) Dependence of the therapeutic success rate with $0.40 \leq r \leq 0.55$ for $0.1 \leq B \leq 0.4$ and $0.4 < B \leq 0.7$ on the number of treatment fractions. Radiation was delivered at 2 Gy/day and 5 days/week in (A) 25 daily fractions or (B and C) increasing number of fractions.

(D) Model-predicted tumor responses to fractionation schemes consisting in 15 and 25 fractions at 2Gy/day and 5 days/week depending on tumor-associated vascularity (B) and the recruitment rate of effector cells in response to tumor burden (r). Tumor control (TC) (blue) and progressive disease (red) refer to tumor eradication and escape after treatment, respectively. Model simulations were performed with $\eta = 8.0 \times 10^5$ cells day^{-1}, $\lambda_M = 1.15$ day^{-1}, and a tumor size at time of RT equal to $R = 15$ mm, unless indicated otherwise.

The remaining parameter values were as in Table S1 [Parameter values considered in model simulations].

of effector cell exhaustion/inactivation caused by prolonged exposure to cancer cells. Increasing tumor burden at time of RT enhances immunogenicity, which results in more efficient antitumor immune responses and favors the recruitment of effector cells to the tumor microenvironment. But at a certain tumor size, insufficient tumor bulk reduction by RT reverts this favorable effect, whereas inactivation of recruited effector cells by their antitumor activity facilitates immune evasion of remaining cancer cells reducing the therapeutic gain. Figure 4D shows that the tumor size b.t. at which larger tumor burden reduction is obtained after RT depends on the functional degrees of tumor vascularity. In tumors of intermediate to low vascularization, disease eradication is more likely in tumors of intermediate size than for smaller and larger tumors. The aforementioned results support that tumor size is not a consistent determinant of therapeutic responses, and suggests that depending on tumor features pre-treatment monitoring of small tumors until they reach a certain critical burden may increase the success rate of fractionated RT.

A One-Size-Fits-All Approach to Conventionally Fractionated Radiotherapy Results in Overtreated Patients

Conventionally fractionated RT is commonly delivered in a one-size-fits-all manner. All cancer patients selected to be treated with this protocol receive about 50 to 70Gy in fractions of 2Gy per day/5 days per week without considering several crucial tumor-specific and microenvironmental factors. Simulations suggest that long fractionation schemes do not significantly improve the therapeutic success rate compared with shorter schemes (Figures 3B and S6 [Impact of treatment duration on tumor control; related to

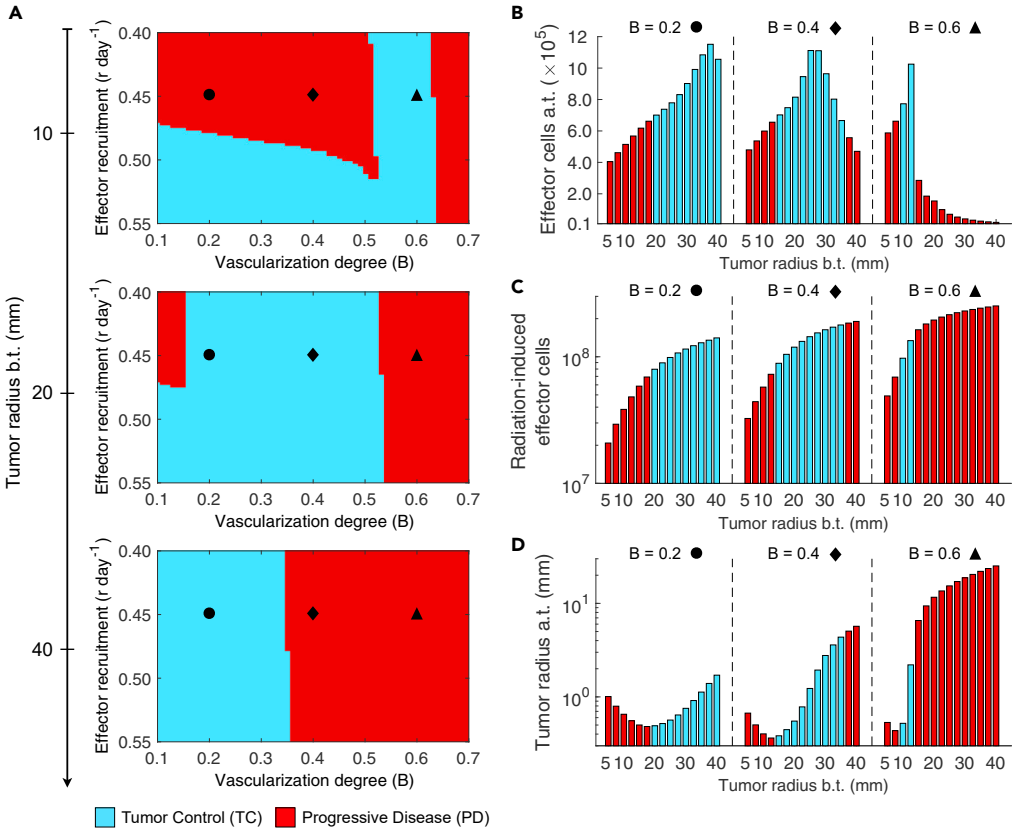

Figure 4. Effect of Tumor Size at Time of RT on Tumor Control and the Tumor-Immune Ecosystem after Treatment

(A) Model-predicted RT responses of tumors with different tumor size before treatment (b.t.), functional degree of tumor-associated vascularity (*B*), and recruitment rates of effector cells in response to tumor burden (*r*).

(B–D) (B) Amount of effector cells and (D) tumor size after treatment (a.t.), and (C) overall radiation-induced effector cells for increasing tumor size before treatment (b.t.) and different values of *B*. Radiation was delivered to a total dose of 50 Gy in 25 daily fractions at 2 Gy per day, 5 days per week. Tumor control (TC) (blue) and progressive disease (red) refer to tumor eradication and escape after treatment, respectively. Model simulations were performed with $\eta = 8.0 \times 10^5$ cells day^{-1} and $\lambda_M = 1.15$ day^{-1}.

The remaining parameter values were as in Table S1 [Parameter values considered in model simulations].

Figure 3]). However, Figure 3C shows that the magnitude of therapeutic gain of increasing the number of treatment fractions depends on the functional degree of tumor-associated vascularity (*B*). The more oxygenated and less hypoxic the tumors are, the better the outcomes with fractionation schemes of increasing number of fractions are. This is due to a continuous tumor burden reduction overcoming tumor cell repopulation favored by oxygen availability. Moreover, treatment duration provides a limited benefit on poorly vascularized tumors by the increased radioresistance of cancer cells under severe hypoxic conditions. These findings suggest that there are several patients receiving higher overall doses than required for tumor eradication or suboptimal fractionation schemes (Figure S6 [Impact of treatment duration on tumor control] and Figure S7 [Treatment duration effect on the tumor-immune ecosystem after radiotherapy]; related to Figure 3). Additionally, Figures S5C and S5D [Intrinsic proliferation and surviving fraction of tumor cells on the therapeutic success rate; related to Figure 3] illustrate the therapeutic success rate dependency on the number of treatment fractions while varying the intrinsic proliferation rate of cancer cells (λ_M) and intrinsic tumor radiosensitivity (i.e., surviving fraction of proliferative and quiescent tumor cells at 2Gy (*Sp*(2Gy) and *Sq*(2Gy) respectively).

Antitumor Immunity Induced by Conventionally Fractionated Radiotherapy Is Mitigated after a Certain Number of Fractions

At first glance, it might seem reasonable that RT fractionation schemes consisting of large number of fractions result in enhanced tumor control. However, radiation does not only kill cancer cells and induces

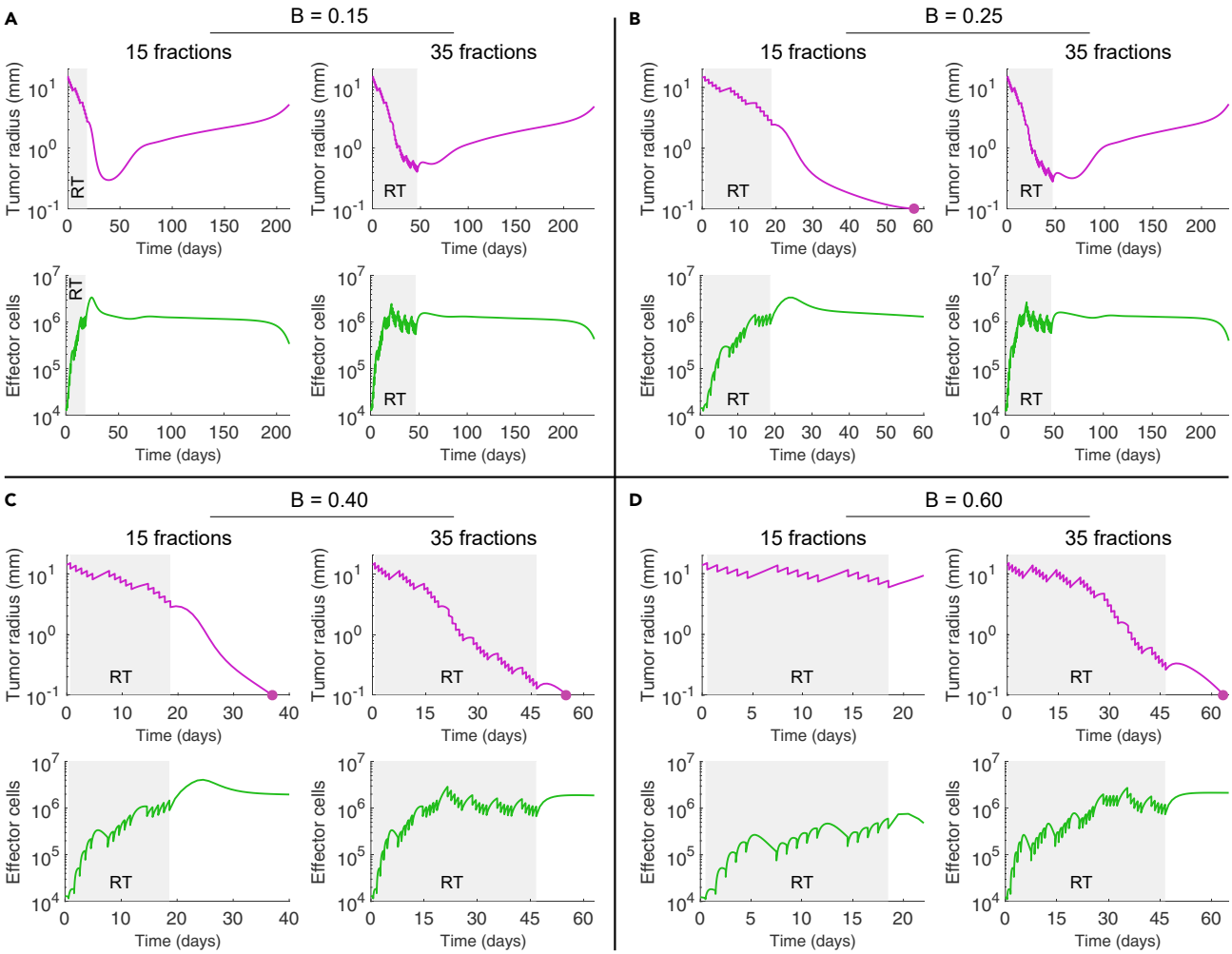

Figure 5. Tumor and Effector Cell Dynamics in Response to RT Fractionation Schemes with Different Number of Fractions

(A–D) Time-evolution of tumor radius and effector cells during and after RT for different functional degrees of tumor-associated vascularity (*B*) and fractionation schemes of 15 and 35 daily fractions at Gy/day and 5 days/week. Model simulations were performed with $\eta = 8.0 \times 10^5$ cells day^{-1}, $\lambda_M = 1.15$ day^{-1}, and a tumor size at time of RT equal to $R = 15$ mm, unless indicated otherwise.

The remaining parameter values were as in Table S1 [Parameter values considered in model simulations].

antitumor immune responses, but also kills tumor-infiltrating effector cells. This not only limits immunogenic tumor cell killing during the course of treatment, but also might result in a more pro-tumoral microenvironment after treatment. Figure 3D shows that an arbitrary increase in treatment duration does not necessarily imply enhanced tumor control. Although some tumors are controlled after 15 fractions at 2.0 Gy/day given 5 days/week, tumor relapse occurs if they are treated with 25 fractions. For tumors with different vascularity degree, Figure 5 shows tumor growth and effector cell dynamics during and after treatments consisting of 15 or 35 fractions (2.0 Gy/day given 5 days/week). Irrespective of tumor control, simulations evidence that after a certain number of fractions the average amount of tumor-infiltrating effector cells decreases (Figures 5A–5C and S7 [Treatment duration effect on the tumor-immune ecosystem after treatment]; related to Figure 3). This mitigation of radiation-induced antitumor immune responses by the direct killing effect of radiation on effector cells leads to less antitumor immunogenic activity at the end of treatment. Although tumor burden reduction is significantly lower when 15 fractions are delivered compared with 35 fractions, a more favorable antitumor environment facilitates immune-mediated tumor elimination at a reduced total dose (Figures 5B, 5C, and S6 [Impact of treatment duration on tumor control]; related to Figure 3). However, Figures 5A and 5D show that long fractionation schemes are needed to treat well-vascularized tumors in order to limit their fast cell repopulation during treatment. Previous results

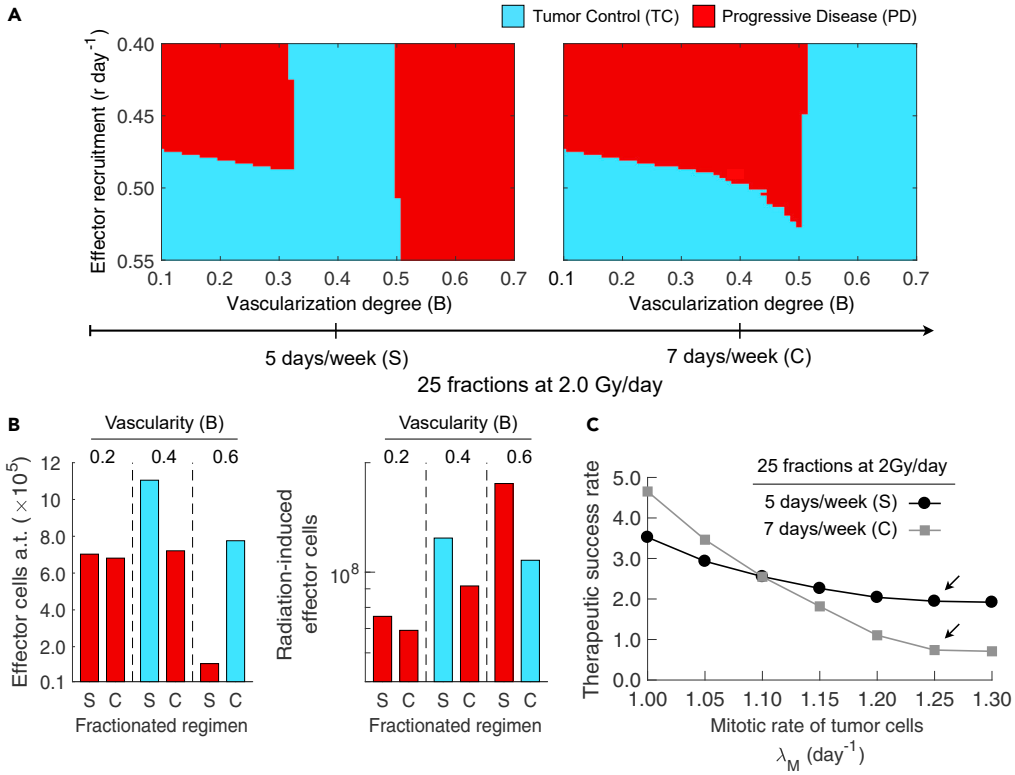

Figure 6. Effect of Weekend Interruptions during RT on Tumor Control and the Tumor-Immune Ecosystem after Treatment

(A) Model-predicted tumor responses to fractionation schemes with and without weekend breaks, depending on the functional degree of tumor-associated vascularity (*B*) and the recruitment rate of effector cells in response to tumor burden (*r*). Radiation was delivered to a total dose of 50 Gy in 25 fractions at 2 Gy/day, (standard; S) 5 days/week, or (consecutive; C) 7 days/week. Tumor control (TC) (blue) and progressive disease (red) refer to tumor eradication and escape after treatment, respectively.

(B) Amount of effector cells at the end of treatment (a.t.) and overall radiation-induced effector cells for tumors with different functional degrees of tumor-associated vascularity (*B*), and treated with the standard (S) or consecutive (C) fractionation scheme.

(C) Dependence of the therapeutic success rate with $0.40 \leq r \leq 0.55$ and $0.1 \leq B \leq 0.5$ on the intrinsic proliferation rate of tumor cells (λ_M) and fractionation protocol of RT. Model simulations were performed with $\eta = 8.0 \times 10^5$ cells day^{-1}, $\lambda_M = 1.25$ day^{-1}, and a tumor size at time of RT equal to $R = 15$ mm, unless indicated otherwise.

The remaining parameter values were as in Table S1 [Parameter values considered in model simulations].

suggest plausibility that depending on tumor-specific features, such as the functional degree of vascularization, shorter fractionation schemes augment immune-mediated tumor cell killing after RT, thus enhancing tumor control probability.

Fractionated Radiotherapy Delivered 5 Days/Week Outperforms Fractionation Schemes Daily Delivered without Weekend Interruptions

Tumor cell repopulation during treatment breaks is an important mechanism commonly associated with treatment failures after RT. This might suggest that fractionation schemes without weekend interruptions decrease the risk of local-regional tumor recurrence. However, simulations predicted that this is not always the case when the underlying radiation-induced immunological processes are taken into account. Figure 6A shows treatment outcomes of fractionation schemes of 25 fractions at 2.0 Gy/day delivered with or without weekend breaks. For poorly to intermediate vascularized tumors ($B \leq 0.5$), tumor cell repopulation during weekend interruptions favored tumor control by an enhanced induction of immunogenic cell death and presence of effector cells after treatment (a.t.) compared with consecutively administered fractions (Figure 6B). In addition, Figure 6B shows that conventional protocols with weekend interruptions result in more overall radiation-induced effector cells irrespective of the functional degree of tumor

vascularity and RT outcomes. This suggests that fractionated RT with weekend interruptions might induce not only stronger local, but also systemic antitumor immunity than the corresponding uninterrupted protocols. On the other hand, Figure 6A also shows that well-vascularized tumors, which are characterized by a significantly faster repopulation rate due to the lack of hypoxia, respond more favorably to consecutive fractions 7 days/week. Moreover, Figure 6B shows that prioritizing burden reduction of well-vascularized tumors (i.e., $B = 0.6$) results in more effector cells in the tumor microenvironment after RT by reducing effector cell inactivation during treatment. Previous results hold irrespective of the strength of radiation-induced antitumor immunity (η). Figure 6C shows that the benefit of weekend breaks 5 days/week over consecutive fractionation schemes 7 days/week on the therapeutic rate of tumors with ($B \leq 0.5$) also depends on the intrinsic proliferation rate of tumor cells. This is due to an increased potential of RT to induce strong antitumor immunity via immunogenic cell death when more tumor cells are killed during treatment.

DISCUSSION

The possibility of intentionally harnessing the synergy of radiation and antitumor immunity promises better treatment outcomes, and it is reflected in some ongoing clinical trials of combined radiation and immunotherapy (Demaria and Formenti, 2016). Although it has become clear that RT enhances tumor immunogenicity (Formenti and Demaria, 2009, 2013; Kaur and Asea, 2012; Roses et al., 2008), especially when promoted with concurrent immunotherapy, the specific contributions of tumor-immune ecosystem components and microenvironmental factors to the local efficacy of radiation-induced antitumor immunity and tumor control remain largely unknown. Moreover, how pre-treatment intrinsic and extrinsic tumor characteristics, as well as immune contexture status, influence systemic antitumor immune response outside the irradiation field (abscopal effect) remains to be elucidated. An improved understanding of the effects of RT on the complex tumor-immune system interplay and underlying dynamics could motivate profound changes in the manner we conceive and clinically prescribe radiotherapy, in particular by understanding radiotherapy as an immunomodulatory therapeutic strategy.

Mathematical modeling provides a valuable testing ground for improving our understanding of complex dynamical systems, such as the immune system and cancer. It has extensively been applied for corroborating hypotheses, generating testable predictions and suggesting unexplored research directions. A diverse set of mathematical models have been proposed to gain mechanistic insights into tumor growth and treatment responses (Enderling et al., 2006, 2010; Powathil et al., 2007; Rockne et al., 2009; Rockne and Frankel, 2017). In addition, several models that describe tumor-immune system interactions have been also reported (de Pillis et al., 2005; d'Onofrio, 2005; Eftimie et al., 2011; Hatzikirou et al., 2015; Hatzikirou et al., 2017; Kuznetsov and Knott, 2001; Matzavinos et al., 2004; Poleszczuk et al., 2016; Ramírez-Torres et al., 2015). Recently, increasing attention has been given to model the synergistic effects of radiotherapy with the immune system. A modeling framework that considers radiation-induced antitumor immunity has been proposed to simulate the evolution of tumor and immune cell populations in anatomically distant metastatic sites (abscopal effect) following surgical resection and RT (Poleszczuk et al., 2016). In the same line, a different model suggested that radiation to the bulk of the tumor could induce a more robust immune response and better harness the synergy of radiotherapy and antitumor immunity than post-surgical radiation to the tumor bed (López-Alfonso et al., 2019). Herein, we presented a mathematical model that focuses on the impact of tumor features such as pre-treatment size, mitotic rate, intrinsic radiosensitivity, and extent of functional degree of tumor-associated vascularity on the immunological consequences of conventionally fractionated RT. Moreover, we investigated the effects of treatment variables such as the number of fractions and weekend interruptions on tumor control probability.

This exploratory study contributes to decipher the complex radiation-immune synergy and provides rationale and motivation for prospective evaluation of the immunogenicity of radiotherapy. According to the model predictions, the functional tumor vascularization extent is a key factor influencing the efficacy of antitumor immunity and tumor response to RT. Simulations suggested that tumor size is not a consistent predictor of treatment outcomes. Although large tumors are more likely to relapse due to an insufficient burden reduction by RT, monitoring small tumors until they reach a certain size could result in more robust radiation-induced antitumor immune responses, thus enhancing tumor control probability. This study is restricted to conventionally fractionated schemes of radiation doses of 2Gy, as it is widely used in clinical practice nowadays (Ahmed et al., 2014). Model analysis revealed that one-size-fits-all approach to conventionally fractionated RT delivering the same number of fractions might result in overtreated patients

receiving doses in excess. The study results suggest plausibility that antitumor immune response induced by fractionated RT could be mitigated after a certain number of fractions depending on the tumor-immune ecosystem features. This result could be explained by the continuous killing effect of radiation on tumor-infiltrating immune cells in radioresistant tumors, which limits the antitumor action of the immune system during and after treatment. The therapeutic benefits of weekend interruptions during the course of conventionally fractionated RT were predicted to depend on tumor-intrinsic features, such as functional degree of vascularity and proliferation rate of cancer cells. Conventional fractionation schemes delivered 5 days/week with weekend interruptions were predicted to generally outperform fractionation schemes delivered 7 days/week.

Although the focus herein was on conventionally fractionated schemes, which are widely used in clinical practice (Ahmed et al., 2014), future work will need to evaluate the impact of different time-dose fractionation schemes on the RT-immune synergy. Emergence of experimental settings and clinical trials that provide data on the immunological consequences of RT is crucial to better calibrate the model parameters and validate modeling predictions. Of utmost importance is to quantitatively measure the effects of radiation dose and delivery frequency on radiation-induced immunogenic cell death and subsequent antitumor immune responses. This information would potentially allow to personalize time-dose fractionation schemes in RT to facilitate adequate immune responses for tumor control. Although theoretical in nature, this *in silico* study suggests therapeutic benefits of profiling patient-specific tumor-immune ecosystems before treatment for enhancing RT-induced antitumor immunity and tumor control. Moreover, modeling findings provide motivation to guide appropriate prospective evaluation of the immunological consequences of radiation-induced cell death.

Limitations of the Study

Model parametrization of tumor-immune system dynamics was based on different tumor growth experiments in immunocompromised and immunocompetent mice. Therefore, calibration on human data and a rigorous evaluation of treatment parameters is essential before clinical translation of the modeling findings.

METHODS

All methods can be found in the accompanying Transparent Methods supplemental file.

DATA AND CODE AVAILABILITY

The data and model implementation code that support the findings of this study are available from the authors on reasonable request.

SUPPLEMENTAL INFORMATION

Supplemental Information can be found online at https://doi.org/10.1016/j.isci.2020.100897.

ACKNOWLEDGMENTS

JCLA, HH, PM and MMH would like to thank the support of the Helmholtz Association of German Research Centers - Initiative and Networking Fund for the project on Reduced Complexity Models 421 (ZT-I-0010). HH would also like to thank the funding support from VolkswagenStiftung (96732). HH, PM and LP are also funded by the BMBF projects MicMode-I2T (01ZX1710B) and MulticellML (01ZX1707C). MMH was in parts supported by the German Federal Ministry of Education and Research within the framework of the e:Med research and funding concept (SysStomach (FKZ: 01ZX1610C)).

AUTHOR CONTRIBUTIONS

JCLA and HH conceived and designed the study. JCLA developed the methodology and performed the model simulations. JCLA, LAP, PM, HH, and MMH structured and analyzed the results. HH and MMH supervised the study. All authors wrote the paper and approved the final version of the manuscript.

DECLARATION OF INTERESTS

The authors declare that no conflict of interests exist.

Received: October 25, 2019
Revised: January 25, 2020
Accepted: February 4, 2020
Published: March 27, 2020

REFERENCES

Ahmed, K.A., Correa, C.R., Dilling, T.J., Rao, N.G., Shridhar, R., Trotti, A.M., Wilder, R.B., and Caudell, J.J. (2014). Altered fractionation schedules in radiation treatment: a review. Semin. Oncol. *41*, 730–750.

Alfonso, J., Buttazzo, G., García-Archilla, B., Herrero, M., and Núñez, L. (2014a). Selecting radiotherapy dose distributions by means of constrained optimization problems. Bull. Math. Biol. *76*, 1017–1044.

Alfonso, L., Carlos, J., Buttazzo, G., García-Archilla, B., Herrero, M.A., and Núñez, L. (2012). A class of optimization problems in radiotherapy dosimetry planning. Discrete Cont. Dyn. Syst. Ser. B *17*, 1651–1672.

Alfonso, J.C.L., Jagiella, N., Núñez, L., Herrero, M.A., and Drasdo, D. (2014b). Estimating dose painting effects in radiotherapy: a mathematical model. PLoS One *9*, e89380.

Atun, R., Jaffray, D.A., Barton, M.B., Bray, F., Baumann, M., Vikram, B., Hanna, T.P., Knaul, F.M., Lievens, Y., Lui, T.Y., et al. (2015). Expanding global access to radiotherapy. Lancet Oncol. *16*, 1153–1186.

Barendsen, G.W., Van Bree, C., and Franken, N.A. (2001). Importance of cell proliferative state and potentially lethal damage repair on radiation effectiveness: implications for combined tumor treatments. Int. J. Oncol. *19*, 247–256.

Barker, H.E., Paget, J.T., Khan, A.A., and Harrington, K.J. (2015). The tumour microenvironment after radiotherapy: mechanisms of resistance and recurrence. Nat. Rev. Cancer *15*, 409.

Begg, A.C., Stewart, F.A., and Vens, C. (2011). Strategies to improve radiotherapy with targeted drugs. Nat. Rev. Cancer *11*, 239–253.

Demaria, S., and Formenti, S.C. (2016). Can abscopal effects of local radiotherapy be predicted by modeling t cell trafficking? J. Immunother. Cancer *4*, 29.

d'Onofrio, A. (2005). A general framework for modeling tumor-immune system competition and immunotherapy: mathematical analysis and biomedical inferences. Phys. D Nonlinear Phenom. *208*, 220–235.

Eftimie, R., Bramson, J.L., and Earn, D.J. (2011). Interactions between the immune system and cancer: a brief review of non-spatial mathematical models. Bull. Math. Biol. *73*, 2–32.

Enderling, H., Anderson, A.R., Chaplain, M.A., Munro, A.J., and Vaidya, J.S. (2006). Mathematical modelling of radiotherapy strategies for early breast cancer. J. Theor. Biol. *241*, 158–171.

Enderling, H., Chaplain, M.A., and Hahnfeldt, P. (2010). Quantitative modeling of tumor dynamics and radiotherapy. Acta Biotheor. *58*, 341–353.

Enderling, H., Alfonso, J.C.L., Moros, E., Caudell, J.J., and Harrison, L.B. (2019). Integrating mathematical modeling into the roadmap for personalized adaptive radiation therapy. Trends Cancer *5*, 467–474.

Formenti, S.C., and Demaria, S. (2009). Systemic effects of local radiotherapy. Lancet Oncol. *10*, 718–726.

Formenti, S.C., and Demaria, S. (2013). Combining radiotherapy and cancer immunotherapy: a paradigm shift. J. Natl. Cancer Inst. *105*, 256–265.

Fridman, W.H., Pagès, F., Sautès-Fridman, C., and Galon, J. (2012). The immune contexture in human tumours: impact on clinical outcome. Nat. Rev. Cancer *12*, 298–306.

Hatzikirou, H., Alfonso, J., Mühle, S., Stern, C., Weiss, S., and Meyer-Hermann, M. (2015). Cancer therapeutic potential of combinatorial immuno- and vasomodulatory interventions. J. R. Soc. Interface *12*, 20150439.

Hatzikirou, H., Alfonso, J.C.L., Leschner, S., Weiss, S., and Meyer-Hermann, M. (2017). Therapeutic potential of bacteria against solid tumors. Cancer Res. *77*, 1553–1563.

Hendry, S.A., Farnsworth, R.H., Solomon, B., Achen, M.G., Stacker, S.A., and Fox, S.B. (2016). The role of the tumor vasculature in the host immune response: implications for therapeutic strategies targeting the tumor microenvironment. Front. Immunol. *7*, 621.

Horsman, M.R., Mortensen, L.S., Petersen, J.B., Busk, M., and Overgaard, J. (2012). Imaging hypoxia to improve radiotherapy outcome. Nat. Rev. Clin. Oncol. *9*, 674–687.

Jain, R.K. (2005). Normalization of tumor vasculature: an emerging concept in antiangiogenic therapy. Science *307*, 58–62.

Kaur, P., and Asea, A. (2012). Radiation-induced effects and the immune system in cancer. Front. Oncol. *2*, 191.

Kuznetsov, V.A., and Knott, G.D. (2001). Modeling tumor regrowth and immunotherapy. Math. Comput. Model. *33*, 1275–1287.

Lee, Y., Auh, S.L., Wang, Y., Burnette, B., Wang, Y., Meng, Y., Beckett, M., Sharma, R., Chin, R., Tu, T., et al. (2009). Therapeutic effects of ablative radiation on local tumor require cd8+ t cells: changing strategies for cancer treatment. Blood *114*, 589–595.

Liu, S., Sun, X., Luo, J., Zhu, H., Yang, X., Guo, Q., Song, Y., and Sun, X. (2015). Effects of radiation on t regulatory cells in normal states and cancer: mechanisms and clinical implications. Am. J. Cancer Res. *5*, 3276.

López-Alfonso, J.C., Poleszczuk, J., Walker, R., Kim, S., Pilon-Thomas, S., Conejo-Garcia, J.J., Soliman, H., Czerniecki, B., Harrison, L.B., and Enderling, H. (2019). Immunologic consequences of sequencing cancer radiotherapy and surgery. JCO Clin. Cancer Inform. *3*, 1–16.

Matzavinos, A., Chaplain, M.A., and Kuznetsov, V.A. (2004). Mathematical modelling of the spatio-temporal response of cytotoxic t-lymphocytes to a solid tumour. Math. Med. Biol. *21*, 1–34.

de Pillis, L.G., Radunskaya, A.E., and Wiseman, C.L. (2005). A validated mathematical model of cell-mediated immune response to tumor growth. Cancer Res. *65*, 7950–7958.

Poleszczuk, J.T., Luddy, K.A., Prokopiou, S., Robertson-Tessi, M., Moros, E.G., Fishman, M., Djeu, J.Y., Finkelstein, S.E., and Enderling, H. (2016). Abscopal benefits of localized radiotherapy depend on activated t-cell trafficking and distribution between metastatic lesions. Cancer Res. *76*, 1009–1018.

Powathil, G., Kohandel, M., Sivaloganathan, S., Oza, A., and Milosevic, M. (2007). Mathematical modeling of brain tumors: effects of radiotherapy and chemotherapy. Phys. Med. Biol. *52*, 3291.

Ramírez-Torres, A., Rodríguez-Ramos, R., Merodio, J., Bravo-Castillero, J., Guinovart-Díaz, R., and Alfonso, J.C.L. (2015). Action of body forces in tumor growth. Int. J. Eng. Sci. *89*, 18–34.

Reppas, A., Alfonso, J., and Hatzikirou, H. (2016). In silico tumor control induced via alternating immunostimulating and immunosuppressive phases. Virulence *7*, 174–186.

Robertson-Tessi, M., El-Kareh, A., and Goriely, A. (2012). A mathematical model of tumor–immune interactions. J. Theor. Biol. *294*, 56–73.

Rockne, R.C., and Frankel, P. (2017). Mathematical modeling in radiation oncology. In Advances in Radiation Oncology, J. Wong, T. Schutheiss, and E. Radany, eds. (Springer), pp. 255–271.

Rockne, R., Alvord, E., Rockhill, J., and Swanson, K. (2009). A mathematical model for brain tumor response to radiation therapy. J. Math.Biol. *58*, 561.

Rockwell, S., Dobrucki, I.T., Kim, E.Y., Marrison, S.T., and Vu, V.T. (2009). Hypoxia and radiation therapy: past history, ongoing research, and future promise. Curr. Mol. Med. *9*, 442–458.

Roses, R.E., Xu, M., Koski, G.K., and Czerniecki, B.J. (2008). Radiation therapy and toll-like receptor signaling: implications for the treatment of cancer. Oncogene *27*, 200–207.

Schaue, D., and McBride, W.H. (2015). Opportunities and challenges of radiotherapy for treating cancer. Nat. Rev. Clin. Oncol. *12*, 527–540.

Serre, R., Benzekry, S., Padovani, L., Meille, C., André, N., Ciccolini, J., Barlesi, F., Muracciole, X., and Barbolosi, D. (2016). Mathematical modeling of cancer immunotherapy and its synergy with radiotherapy. Cancer Res. *76*, 4931–4940.

Sharma, R.A., Plummer, R., Stock, J.K., Greenhalgh, T.A., Ataman, O., Kelly, S., Clay, R., Adams, R.A., Baird, R.D., Billingham, L., et al. (2016). Clinical development of new drug-radiotherapy combinations. Nat. Rev. Clin. Oncol. *13*, 627–642.

Thariat, J., Hannoun-Levi, J.-M., Myint, A.S., Vuong, T., and Gérard, J.-P. (2013). Past, present, and future of radiotherapy for the benefit of patients. Nat. Rev. Clin. Oncol. *10*, 52–60.

Wilkie, K.P. (2013). A review of mathematical models of cancer–immune interactions in the context of tumor dormancy. In Systems Biology of Tumor Dormancy. Advances in Experimental Medicine and Biology, *734*, H. Enderling, N. Almog, and L. Hlatky, eds (Springer), pp. 201–234.

iScience, Volume *23*

Supplemental Information

On the Immunological Consequences of Conventionally Fractionated Radiotherapy

Juan Carlos L. Alfonso, Lito A. Papaxenopoulou, Pietro Mascheroni, Michael Meyer-Hermann, and Haralampos Hatzikirou

Transparent Methods

A model of tumor-effector cells response to radiotherapy

We further develop a previous model of tumor-effector cell interactions, calibrated on the basis of murine tumor growth data (Hatzikirou et al. 2015), to investigate the potential benefits and effects of radiotherapy (RT) on antitumor immune responses. We refer the readers to (Hatzikirou et al. 2017, 2015, Reppas et al. 2016) for further details on model formulation, implementation and applications, as well as on parameter calibration and theoretical analysis. The main novelty of the extended model is the simulation of the immunological consequences of RT by considering the radiation-induced antitumor immunity and subsequent tumor-immune system dynamics. Modeling of RT relies on experimental and clinical evidence concerning the radiation effects on both tumor cells and the immune system. It is well known that radiation effectively kills not only tumor cells, but also tumor-infiltrating immune cells at different rates (Belka et al. 1998, Prise & O'sullivan 2009). Radiation-induced cell killing mostly occurs as a result of DNA single and double strand breaks in individual cells, followed by some forms of cell death (Golden et al. 2012, Maier et al. 2016). Accumulating evidence has shown that reduced oxygen availability is one of the main microenvironmental factors contributing to tumor radioresistance (Brown 1999), with poorly-oxygenated (hypoxic, and generally quiescent) tumor cells being more radioresistant than cycling (normoxic) tumor cells (Barendsen et al. 2001, Moeller et al. 2007, Pawlik & Keyomarsi 2004, Rockwell et al. 2009). Recently, it has been also shown that exposure to radiation induces dying tumor cells to express significantly more tumor-associated antigens on their surface and to release damage-associated molecular patterns, i.e. immunostimulatory danger signals, which then are taken up and processed by professional antigen presenting cells (APCs, i.e., dendritic cells). Activated APCs migrate to proximal lymph nodes and activate tumor-specific effector cells, resulting in an adaptive local and systemic immune response (Demaria & Formenti 2016, Formenti & Demaria 2009, Kaur & Asea 2012, Vatner et al. 2014, Weichselbaum et al. 2017). Figure 1(A) shows a schematic view of RT-induced immune modulations.

The model of cancer treatment by RT considering tumor-effector cell interactions is given by the following system of ordinary differential equations

$$\frac{dR}{dt} = \frac{1}{3}(\lambda_M B - \lambda_A)R + \lambda_M(1-B)L\left(\frac{1}{\tanh(R/L)} - \frac{L}{R}\right) - cER\,f(R,B), \tag{S1}$$

$$\frac{dE}{dt} = r\frac{R^3}{K+R^3}E + \eta\frac{D^3}{M+D^3} - d_1R^3E\,f(R,B) - d_0E + \sigma, \tag{S2}$$

$$\frac{dD}{dt} = -\theta D, \tag{S3}$$

where $R(t)$ is the tumor radius, $E(t)$ is the effector cell concentration in the tumor microenvironment and $D(t)$ is the radius corresponding to the spherical tumor volume reduced by radiation. Time coordinate t has been omitted in Eqs. (S1)-(S3) for sake of notation simplicity. Figure 1(B) shows a schematic representation of the interactions between the model components, and Table S1 summarizes the meaning of model parameters with their values used in model simulations.

The first and second terms of Eq. (S1) represent vascular and avascular tumor growth, where $0 \leq B \leq 1$ is a dimensionless parameter that represents the functional degree of tumor-associated vascularity, i.e., blood vessels within tumors that supply oxygen and permit immune cell extravasation, modulating both tumor growth and tumor-effector cell interactions. The limit $B = 0$ represents completely avascular tumors, while $B = 1$ corresponds to fully-vascularized tumors. For model simulations, we set $0.1 \leq B \leq 0.7$ as neither avascular nor fully-vascularized tumors are realistic situations in the clinical setting. We assumed that in poorly-vascularized tumors with $B \approx 0.1$ tumor-effector cell interactions mainly take place at the tumor surface, while in well-vascularized tumors $B \approx 0.7$ effector cells can potentially interact with any cancer cell within the tumor bulk. We notice that, values of B close to 0.7 correspond to

Symbol	Parameter Description	Value	Unit	Source
λ_M	Intrinsic proliferation rate of tumor cells	[1.15 - 1.30]	day^{-1}	(Alessandri et al. 2013) (Delarue et al. 2013)
λ_A	Death rate of tumor cells	1.4×10^{-1}	day^{-1}	(Hatzikirou et al. 2015)
L	Characteristic nutrient diffusion length	2.9×10^{-1}	mm	(Hatzikirou et al. 2015)
c	Killing rate of tumor cells by effector cells	3.0×10^{-2}	$\text{cells}^{-1}\ \text{day}^{-1}$	(Hatzikirou et al. 2015)
r	Recruitment rate of effector cells in response to tumor burden	[0.40 - 0.55]	day^{-1}	(Hatzikirou et al. 2015)
K	Antitumor immunostimulation damping coefficient	2.72	mm^3	(Kuznetsov et al. 1994) (de Pillis et al. 2005) (dOnofrio 2005) (d'Onofrio et al. 2012)
d_1	Inactivation rate of effector cells by their antitumor activity	10^{-2}	$\text{mm}^{-3}\ \text{day}^{-1}$	(Kuznetsov et al. 1994) (de Pillis et al. 2005) (dOnofrio 2005)
d_0	Death rate of effector cells	3.7×10^{-1}	day^{-1}	(Kuznetsov & Knott 2001) (dOnofrio 2005) (Su et al. 2009) (d'Onofrio et al. 2012)
σ	Baseline recruitment of effector cells	0.13×10^5	cells day^{-1}	(Kuznetsov et al. 1994) (de Pillis et al. 2005) (dOnofrio 2005) (d'Onofrio et al. 2012)
B	Functional degree of tumor vascularity	[0.1 - 0.7]	Dimensionless	*Assumed*
η	Radiation-induced antitumor immunostimulation	$[5.0, 10.0] \times 10^5$	cells day^{-1}	*Assumed*
M	Radiation-induced antitumor immunostimulation damping coefficient	10^3	mm^3	*Assumed*
θ	Decay rate of radiation-induced immunostimulatory signals	10^{-2}	day^{-1}	*Assumed*
α	Radiation sensitivity parameter	0.294	Gy^{-1}	(Leith et al. 1991)
β	Radiation sensitivity parameter	0.0603	Gy^{-2}	(Leith et al. 1991)
ξ	Tumor cell radiation resistance for proliferating cells	1	Dimensionless	(Enderling et al. 2009) (Alfonso et al. 2014)
ξ	Tumor cell radiation resistance for quiescent cells	1/3	Dimensionless	(Enderling et al. 2009) (Alfonso et al. 2014)

Table S1: **Parameter Values Considered in Model Simulations.** [Related to Figure 1]. These values are used unless indicated otherwise.

fast-growing tumors with a functional degree of tumor vascularization close to normal, which can only be reached by therapeutic strategies such as normalization or stress alleviation (Jain 2005, Stylianopoulos et al. 2012). The mitotic and death rates of tumor cells are given by λ_M and λ_A, respectively. The parameter L represents the intrinsic length scale resulting from nutrient dynamics, i.e., diffusion, supply

and consumption (Hatzikirou et al. 2015). The last term of Eq. (S1) models immunocompetent effector cell-mediated killing of tumor cells at a rate c as part of adaptive immune responses. The expression $f(R,B) = \frac{R^{(B-1)}}{R^{(B-1)}+1}$, is a phenomenological scaling function that models the infiltration of effector cells into the tumor bulk through the functional tumor vasculature (Hatzikirou et al. 2015). This function modulates tumor-effector cell interactions in Eq. (S1) and inactivation of effectors owing to their antitumor activity in Eq. (S2).

The first term of Eq. (S2) refers to the recruitment of effector cells into the tumor microenvironment in response to tumor burden at a rate r following Michaelis-Menten dynamics, where K is the antitumor immunostimulation damping coefficient representing the tumor volume at which the recruitment rate r is half-maximal. We assumed that immune cells are recruited in response to signals released from both tumor cells and immunogenic dying cells as a result of severe hypoxic conditions and antitumor immune responses. The second term of Eq. (S2) follows Michaelis-Menten dynamics and it is related to the recruitment of effector cells at a rate η resulting from RT-induced immunostimulatory signals from dying tumor cells. The parameter M is the RT-induced antitumor immunostimulation damping coefficient at which η is half-maximal. The strength of RT-induced antitumor immune responses, characterized by subsequent infiltration of effector cells into the tumor bed, was assumed to depend on the radiation-mediated tumor radius reduction representing the dying tumor cells undergoing immunogenic cell death that emits immunostimulating signals and chemokines. The last three terms of Eq. (S2) respectively simulate the exhaustion/inactivation of effector cells by their antitumor activity at a rate d_1, the spontaneous apoptotic effector cell death at a rate d_0 and baseline immunosurveillance σ, i.e., the baseline presence of effector cells at any time (immunosurveillance) even in the absence of tumor cells. Eq. (S3) describes the decay of radiation-induced immunostimulatory signals at a rate θ.

Radiation effect on tumors

The cytotoxic effect of RT on tumors was simulated using the linear-quadratic (LQ) model, the most widely used dose-response formulation in RT (Brenner 2008, Fowler 1989, Lee et al. 1995). According to the LQ model, the surviving fraction (S) of tumor cells receiving a radiation dose d [Gy] is given by

$$S(d) = \mathrm{e}^{-\xi(\alpha d+\beta d^2)} \tag{S4}$$

where the dose coefficients α [Gy^{-1}] and β [Gy^{-2}] are tumor type-specific radiosensitivity parameters, and ξ is a parameter used to distinguish the different radiosensitivities of proliferative and hypoxic tumor cells (Alfonso et al. 2014, Enderling et al. 2009). We used $\alpha = 0.294$ Gy^{-1} and $\beta = 0.0603$ Gy^{-2} as estimated from 20 colon cancer cell lines (Leith et al. 1991), because the model of tumor-effector cell interactions in Eqs. (S1)-(S3) was calibrated from *in vivo* experiments of murine CT26 (mouse colon carcinoma cell line) tumor growth, see (Hatzikirou et al. 2015) for further details. Compelling evidence demonstrates that hypoxic (poorly-oxygenated) tumor cells are quiescent and estimated to be approximately three-times more radioresistant than normoxic cycling cells (Moeller et al. 2007, Rockwell et al. 2009). Accordingly, we set $\xi = 1$ for proliferating tumor cells $S_p(d)$, and $\xi = 1/3$ for quiescent tumor cells $S_q(d)$ (Alfonso et al. 2014, Enderling et al. 2009). The probabilities of surviving 2Gy of radiation were $S(2\mathrm{Gy}) = 0.44$ for proliferating cancer cells ($\xi = 1$) and $S(2\mathrm{Gy}) = 0.76$ for quiescent cancer cells ($\xi = 1/3$). Thus, tumor radiosensitivity is determined by the intrinsic radiosensitivity of tumor cells (i.e., α and β parameters of the LQ model), and modulated by microenvironmental conditions such as hypoxia (i.e., parameter ξ in Eq. (S4)).

Hypoxia-mediated radioresistance was modeled by considering tumors divided into an outer vascularized layer of thickness BR and an inner avascular region of radius $(1-B)R$, where R is the tumor radius and B is the functional degree of tumor vascularity. In addition, the inner avascular region structurally consists of a proliferative rim (δ_p), an intermediate hypoxic/quiescent region (δ_q) and a central necrotic core of radius R_N. The thickness of the avascular proliferative rim δ_p is determined by the diffusion

of oxygen from the surrounding functional blood vessels in the outer vascularized tumor region. The central necrotic core is separated from the proliferating rim by a poorly-oxygenated layer of thickness δ_q, in which tumor cells are hypoxic and not undergoing cell division. Accordingly, $(BR + \delta_p)$ and δ_q represent the overall proliferative and quiescent tumor regions, respectively. In the model, tumors grow with $\delta_p = b((1-B)R)^{2/3}$ and $\delta_q = a((1-B)R)^{2/3}$, where $(1-B)R$ is the radius of the inner avascular region. The radius of necrotic core R_N is $(1-B)R - \delta_p - \delta_q$ resulting in smaller necrotic cores with functional degree of tumor vascularity. Based on experimental data, estimates of δ_p and δ_q have been used to model avascular tumor growth (Kansal et al. 2000, Schmitz et al. 2002). It has been reported that $\delta_p = bR^{2/3}$ and $\delta_q = aR^{2/3}$ with $b = 0.11$ mm$^{1/3}$ and $a = 0.42$ mm$^{1/3}$, where the two-thirds power law reflects a surface-to-volume ratio that can be biologically interpreted as oxygen diffusing through the tumor surface. Figure 1(C) shows a cross sectional view of the structure of simulated spherical tumors.

At each treatment fraction of dose d at time $t = \tau_i$, the radiation-induced change in the tumor radius R in Eq. (S1) is given by

$$R^* = \left[\frac{3}{4\pi}\Big(S_p(d)V_p + S_q(d)V_q + V_n\Big)\right]^{1/3} \tag{S5}$$

where R^* is the tumor radius at the time instant after τ_i. Using the LQ model in Eq. (S4), the surviving fractions of proliferating and quiescent tumor cells are given by $S_p(d)V_p$ and $S_q(d)V_q$, where $V_p = \big[V_c - \frac{4}{3}\pi((1-B)R - \delta_p)^3\big]$, $V_q = \big[\frac{4}{3}\pi((1-B)R - \delta_p)^3 - V_n\big]$, $V_n = \frac{4}{3}\pi R_N^3$ and $V_c = \frac{4}{3}\pi R^3$ are the volumes of the proliferative tumor region, the quiescent tumor region, the necrotic core and the whole tumor, respectively (Figure 1(C)). At the time instant after τ_i, $D^* = D + (R - R^*)$ is the contribution to the strength of radiation-induced antitumor immune responses determined by $D(t)$ in Eq. (S3).

Radiation effect on effector cells

At each treatment fraction of dose d at time $t = \tau_i$, the radiation-induced change in the concentration of effector cells in the tumor microenvironment (E) in Eq. (S2) is given by

$$E^* = S_E(d)E \tag{S6}$$

where E^* is the concentration of tumor-infiltrating effector cells at the time instant after τ_i. Using the LQ model in Eq. (S4), $S_E(d)$ is the surviving fraction of effector cells receiving a radiation dose d. Effector cell radiosensitivity was estimated on the basis of experimental data of radiation-induced apoptosis in lymphocytes obtained from blood samples (Schnarr et al. 2007). Experimental evidence supports that apoptosis is one of the dominant cell death processes of lymphocytes in response to RT (Dewey et al. 1995), and correlation between the intensity of apoptosis in lymphocytes and radiation dose has been reported (Cui et al. 1999, Schnarr et al. 2007). From dose-response curves of effector CD8$^+$ T cells *in vitro* after exposure to acute doses of 0 to 8 Gy, we derived $S_E(2\text{Gy}) = 0.61$.

Therapeutic success rate

The therapeutic success rate is defined as the ratio of controlled tumors after radiotherapy to all the treated tumors with respect to certain ranges of the functional degree of tumor-associated vascularity (B) and the recruitment rate of effector cells in response to tumor burden (r).

Model simulations and treatment delivery

For demonstration purposes, we considered model parameter values that simulate growing tumors in the absence of RT (Table S1). For analysis, we changed model parameters that may represent the patient-specific biology of individual patients. RT was simulated with a total dose of 50 Gy delivered in 25 daily fractions at 2Gy/day and 5 days/week, unless indicated otherwise. The total dose of 50Gy was chosen

for demonstration purposes in line with conventionally fractionated (standard) protocols used to treat a wide range of cancer types (Ahmed et al. 2014). Model simulations were initialized with a tumor radius of 0.1 mm, 0.13×10^5 effector cells (baseline presence) and no radiation-induced antitumor immunostimulation, see Eqs. (S1)-(S3). These initial conditions result in tumor escape immunosurveillance, and allow to then simulate the effector of RT. The sensitivity analysis of the model in Eqs. (S1)-(S3) without RT can be found in (Hatzikirou et al. 2015, Reppas et al. 2016), where we provided phase portrait diagrams and performed the bifurcation analysis. In this study, we extended that model by considering the effects of RT, which only impacts the post-treatment system dynamics and not the stability of the fixed points. Simulated tumors reaching a certain pre-defined size were treated with RT and assumed to be controlled after RT if their radii are reduced until reaching either 10^{-2} mm or the necrotic core radius, i.e., no viable tumor cells present. In the case of progressive disease after RT, simulations continued until tumors reached the pre-treatment size. The delivery of each RT fraction and subsequent responses to radiation of both effector and tumor cells were assumed instantaneous, i.e., faster than the cell-cycle duration. The mathematical model was implemented and simulated in Matlab (*www.mathworks.com*).

Supplemental Figures

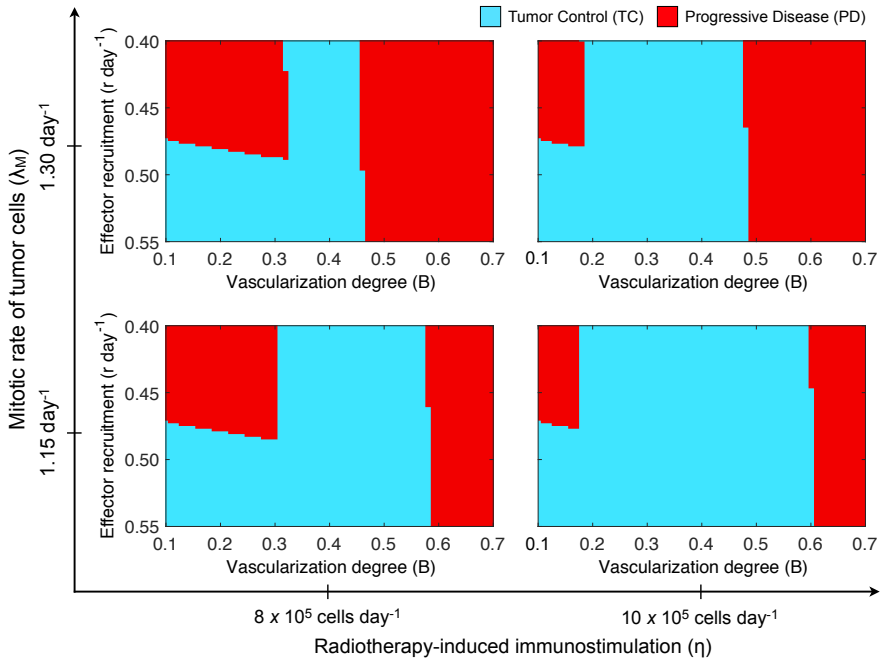

Figure S1: **Tumor Vascularity and Effector Cell Recruitment on Response to Radiotherapy.** [Related to Figure 2]. Effect of functional tumor vascularity (B) and recruitment rate of effector cells in response to tumor burden (r) on tumor response to RT for different strengths of tumor-specific immunity induced by radiation (η) and intrinsic mitotic rates of tumor cells (λ_M). Radiation was delivered to a total dose of 50 Gy in 25 daily fractions at 2 Gy per day, 5 days per week. Tumor control (TC) (blue) and progressive disease (red) refer to tumor eradication and tumor escape after treatment, respectively. Model simulations were performed with a tumor size at time of RT equal to $R = 15$ mm. The remaining parameter values were as in Table S1.

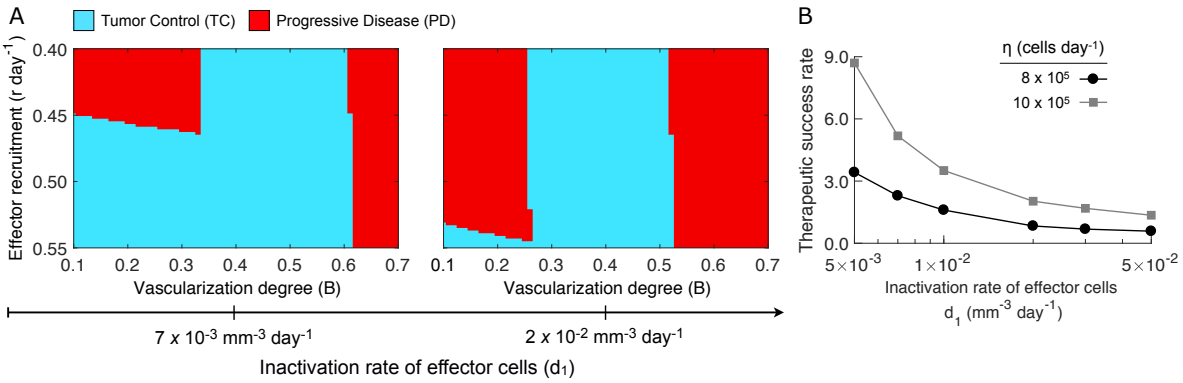

Figure S2: **Inactivation Rate of Effector Cells on Tumor Response to Radiotherapy and Therapeutic Success Rate.** [Related to Figure 2]. **(A)** Model-predicted tumor responses to RT depending on the functional degree of tumor-associated vascularity (B) and the recruitment rate of effector cells in response to tumor burden (r). **(B)** Dependence of the therapeutic success rate with $0.40 \leq r \leq 0.55$ and $0.1 \leq B \leq 0.7$ on the strength of radiation-induced antitumor immune responses (η) and inactivation rate of effector cells d_1. Radiation was delivered to a total dose of 50 Gy in 25 daily fractions at 2 Gy per day, 5 days per week. Tumor control (TC) (blue) and progressive disease (red) refer to tumor eradication and escape after treatment, respectively. Model simulations were performed with $\eta = 8.0 \times 10^5$ cells day^{-1}, $\lambda_M = 1.15$ day^{-1} and a tumor size at time of RT equal to $R = 15$ mm. The remaining parameter values were as in Table S1.

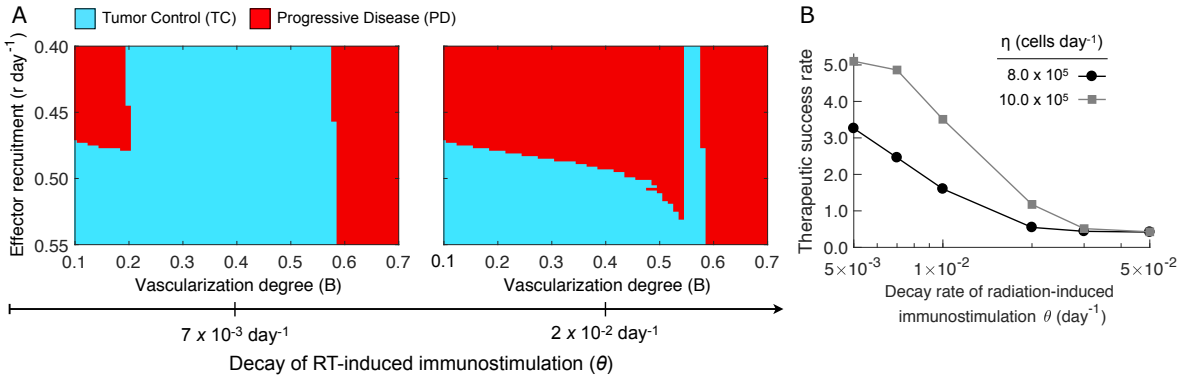

Figure S3: **Decay of Radiation-induced Immunostimulation on Tumor Response to Radiotherapy and Therapeutic Success Rate.** [Related to Figure 2]. **(A)** Model-predicted tumor responses to RT depending on the functional degree of tumor-associated vascularity (B) and the recruitment rate of effector cells in response to tumor burden (r). **(B)** Dependence of the therapeutic success rate with $0.40 \leq r \leq 0.55$ and $0.1 \leq B \leq 0.7$ on the strength of radiation-induced antitumor immune responses (η) and the decay rate of RT-induced immunostimulatory signals θ. Radiation was delivered to a total dose of 50 Gy in 25 daily fractions at 2 Gy per day, 5 days per week. Tumor control (TC) (blue) and progressive disease (red) refer to tumor eradication and escape after treatment, respectively. Model simulations were performed with $\eta = 8.0 \times 10^5$ cells day^{-1}, $\lambda_M = 1.15$ day^{-1} and a tumor size at time of RT equal to $R = 15$ mm. The remaining parameter values were as in Table S1.

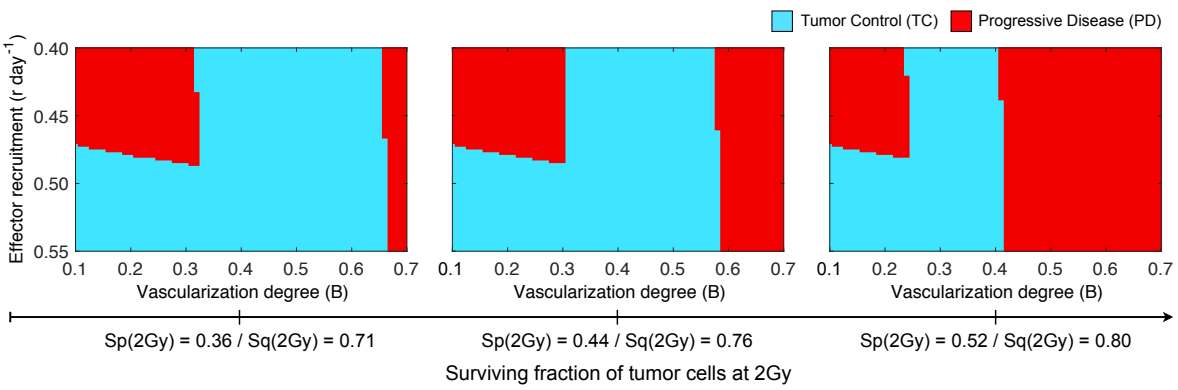

Figure S4: **Intrinsic Cancer Cell Radiosensitivity on Tumor Response to Radiotherapy.** [Related to Figure 2]. Model-predicted tumor responses to RT depending on the functional degree of tumor-associated vascularity and the recruitment rate of effector cells in response to tumor burden (r) for different surviving fractions of tumor cells at 2Gy ($S_p(2\text{Gy})$ for proliferating tumor cells and $S_q(2\text{Gy})$ for quiescent tumor cells). Radiation was delivered to a total dose of 50 Gy in 25 daily fractions at 2 Gy per day, 5 days per week. Tumor control (TC) (blue) and progressive disease (red) refer to tumor eradication and escape after treatment, respectively. Model simulations were performed with $\eta = 8.0\times10^5$ cells day^{-1}, $\lambda_M = 1.15$ day^{-1} and a tumor size at time of RT equal to $R = 15$ mm. The remaining parameter values were as in Table S1.

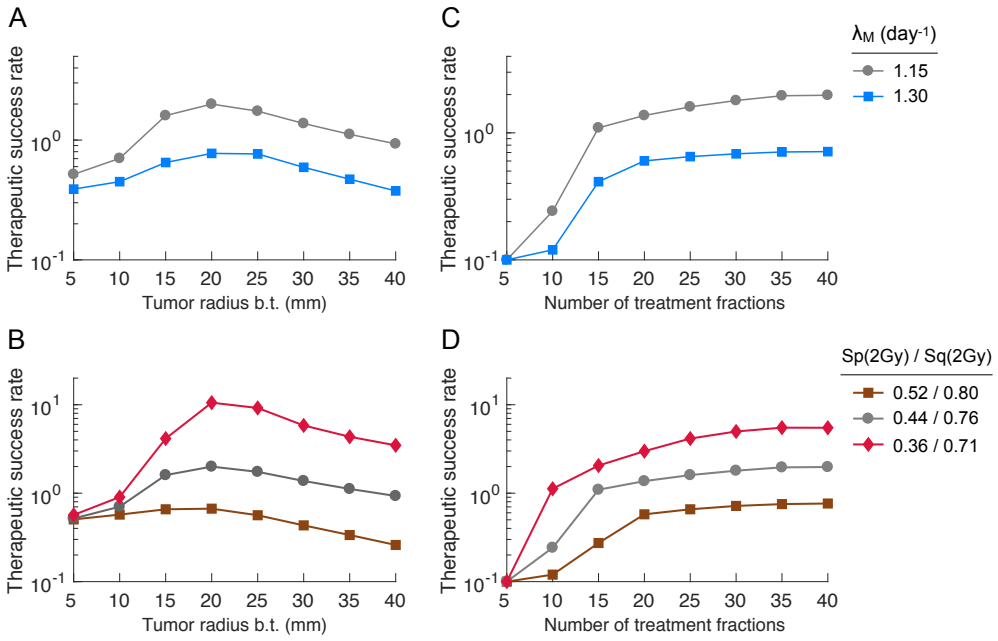

Figure S5: **Intrinsic Proliferation and Surviving Fraction of Tumor Cells on the Therapeutic Success Rate.** [Related to Figures 3]. Dependence of RT outcomes on the intrinsic proliferation rate of tumor cells (λ_M) and surviving fraction of tumor cells at 2Gy for increasing tumor size before treatment (b.t.) and number of treatment fractions. S_p(2Gy) and S_q(2Gy) represent the surviving fraction of proliferating and quiescent tumor cells receiving 2Gy. Radiation was delivered at 2 Gy/day and 5 days/week in **(A,B)** 25 daily fractions and **(C,D)** for increasing number of fractions. Model simulations were performed with $\eta = 8.0 \times 10^5$ cells day^{-1}, $\lambda_M = 1.15$ day^{-1} and a tumor size at time of RT equal to $R = 15$ mm, unless indicated otherwise. The remaining parameter values were as in Table S1.

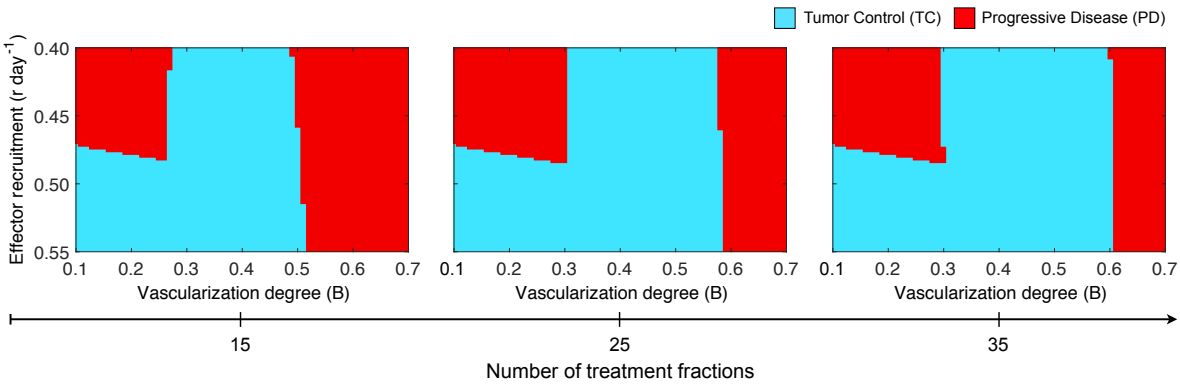

Figure S6: **Impact of Treatment Duration on Tumor Control.** [Related to Figure 3]. Effect of functional tumor vascularity (B) and recruitment rate of effector cells in response to tumor burden (r) on response to fractionation schemes consisting in different number of treatment fractions. Radiation was delivered to a total dose of 50 Gy in 25 daily fractions at 2 Gy per day, 5 days per week. Tumor control (TC) (blue) and progressive disease (red) refer to tumor eradication and escape after treatment, respectively. Model simulations were performed with $\eta = 8.0 \times 10^5$ cells day^{-1}, $\lambda_M = 1.15$ day^{-1} and a tumor size at time of RT equal to $R = 15$ mm. The remaining parameter values were as in Table S1.

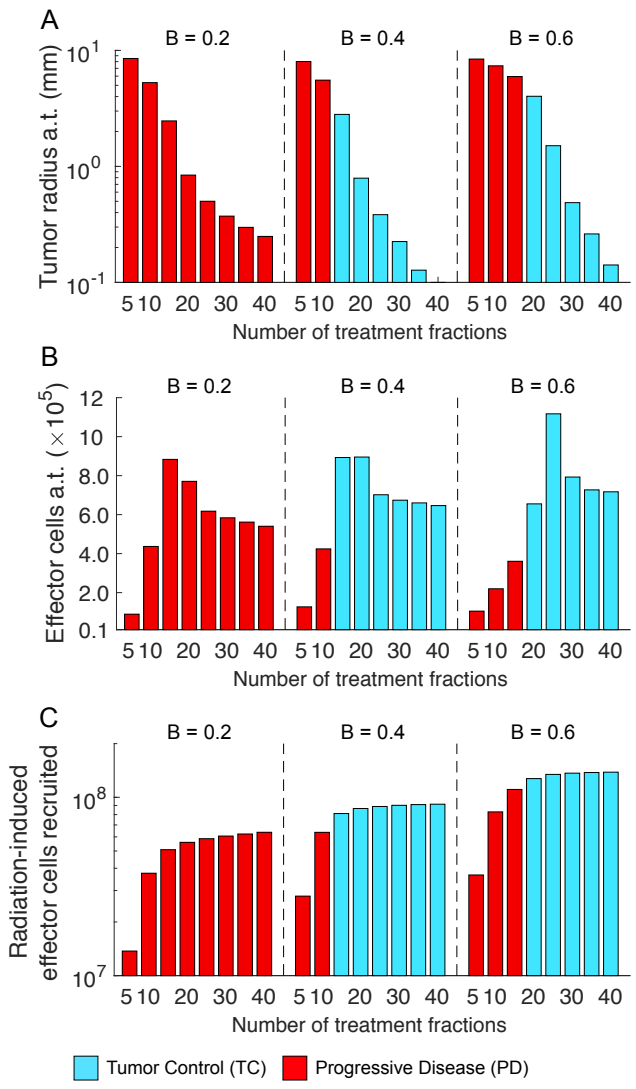

Figure S7: **Treatment Duration Effect on the Tumor-Immune Ecosystem after Radiotherapy.** [Related to Figure 3]. **(A)** Tumor size and **(B)** amount of effector cells after treatment (a.t.), and **(C)** overall radiation-induced effector cells for tumors of different functional degrees of tumor-associated vascularity (B) and treated with fractionation schemes of increasing number of fractions. Radiation was delivered at 2 Gy/day and 5 days/week in increasing number of fractions. Tumor control (TC) (blue) and progressive disease (red) refer to tumor eradication and escape after treatment, respectively. Model simulations were performed with $\eta = 8.0 \times 10^5$ cells day^{-1}, $\lambda_M = 1.15$ day^{-1} and a tumor size at time of RT equal to $R = 15$ mm. The remaining parameter values were as in Table S1.

Supplemental References

Ahmed, K. A., Correa, C. R., Dilling, T. J., Rao, N. G., Shridhar, R., Trotti, A. M., Wilder, R. B. & Caudell, J. J. (2014), 'Altered fractionation schedules in radiation treatment: a review', *Seminars in oncology* **41**(6), 730–750.

Alessandri, K., Sarangi, B., Gurchenkov, V., Sinha, B., Kießling, T., Fetler, L., Rico, F., Scheuring, S., Lamaze, C., Simon, A., Geraldo, S., Vignjevic, D., Doméjean, H., Rolland, L., Funfak, A., Bibette, J., Bremond, N. & Nassoy, P. (2013), 'Cellular capsules as a tool for multicellular spheroid production and for investigating the mechanics of tumor progression in vitro', *Proc Natl Acad Sci U S A* **110**(37), 14843–14848.

Alfonso, J. C. L., Jagiella, N., Núñez, L., Herrero, M. A. & Drasdo, D. (2014), 'Estimating dose painting effects in radiotherapy: a mathematical model', *PloS one* **9**(2), e89380.

Barendsen, G. W., Van Bree, C. & Franken, N. A. (2001), 'Importance of cell proliferative state and potentially lethal damage repair on radiation effectiveness: implications for combined tumor treatments', *International journal of oncology* **19**(2), 247–256.

Belka, C., Marini, P., Budach, W., Schulze-Osthoff, K., Lang, F., Gulbins, E. & Bamberg, M. (1998), 'Radiation-induced apoptosis in human lymphocytes and lymphoma cells critically relies on the up-regulation of cd95/fas/apo-1 ligand', *Radiation research* **149**(6), 588–595.

Brenner, D. J. (2008), 'The linear-quadratic model is an appropriate methodology for determining isoeffective doses at large doses per fraction', *Seminars in radiation oncology* **18**(4), 234–239.

Brown, J. M. (1999), 'The hypoxic cell', *Cancer research* **59**(23), 5863–5870.

Cui, Y., Gao, Y., Yang, H., Xiong, C., Xia, G. & Wang, D. (1999), 'Apoptosis of circulating lymphocytes induced by whole body gamma-irradiation and its mechanism.', *Journal of environmental pathology, toxicology and oncology: official organ of the International Society for Environmental Toxicology and Cancer* **18**(3), 185–189.

de Pillis, L. G., Radunskaya, A. E. & Wiseman, C. L. (2005), 'A validated mathematical model of cell-mediated immune response to tumor growth', *Cancer research* **65**(17), 7950–7958.

Delarue, M., Montel, F., Caen, O., Elgeti, J., Siaugue, J., Vignjevic, D., Prost, J., Joanny, J. & Cappello, G. (2013), 'Mechanical control of cell flow in multicellular spheroids', *Phys Rev Lett* **110**(13), 138103.

Demaria, S. & Formenti, S. C. (2016), 'Can abscopal effects of local radiotherapy be predicted by modeling t cell trafficking?', *Journal for immunotherapy of cancer* **4**(1), 29.

Dewey, W. C., Ling, C. C. & Meyn, R. E. (1995), 'Radiation-induced apoptosis: relevance to radiotherapy', *International Journal of Radiation Oncology* Biology* Physics* **33**(4), 781–796.

d'Onofrio, A., Ledzewicz, U. & Schättler, H. (2012), On the dynamics of tumor-immune system interactions and combined chemo-and immunotherapy, *in* 'In New Challenges for Cancer Systems Biomedicine. SIMAI Springer Milan', Springer, pp. 249–66.

dOnofrio, A. (2005), 'A general framework for modeling tumor-immune system competition and immunotherapy: Mathematical analysis and biomedical inferences', *Physica D: Nonlinear Phenomena* **208**(3), 220–235.

Enderling, H., Park, D., Hlatky, L. & Hahnfeldt, P. (2009), 'The importance of spatial distribution of stemness and proliferation state in determining tumor radioresponse', *Mathematical Modelling of Natural Phenomena* **4**(3), 117–133.

Formenti, S. C. & Demaria, S. (2009), 'Systemic effects of local radiotherapy', *The lancet oncology* **10**(7), 718–726.

Fowler, J. F. (1989), 'The linear-quadratic formula and progress in fractionated radiotherapy', *The British journal of radiology* **62**(740), 679–694.

Golden, E. B., Pellicciotta, I., Demaria, S., Barcellos-Hoff, M. H. & Formenti, S. C. (2012), 'The convergence of radiation and immunogenic cell death signaling pathways', *Frontiers in oncology* **2**.

Hatzikirou, H., Alfonso, J. C. L., Leschner, S., Weiss, S. & Meyer-Hermann, M. (2017), 'Therapeutic potential of bacteria against solid tumors', *Cancer Research* **77**(7), 1553–1563.

Hatzikirou, H., Alfonso, J., Mühle, S., Stern, C., Weiss, S. & Meyer-Hermann, M. (2015), 'Cancer therapeutic potential of combinatorial immuno-and vasomodulatory interventions', *Journal of The Royal Society Interface* **12**(112), 20150439.

Jain, R. K. (2005), 'Normalization of tumor vasculature: an emerging concept in antiangiogenic therapy', *Science* **307**(5706), 58–62.

Kansal, A. R., Torquato, S., Harsh, G., Chiocca, E. & Deisboeck, T. (2000), 'Simulated brain tumor growth dynamics using a three-dimensional cellular automaton', *Journal of theoretical biology* **203**(4), 367–382.

Kaur, P. & Asea, A. (2012), 'Radiation-induced effects and the immune system in cancer', *Frontiers in oncology* **2**(191).

Kuznetsov, V. A. & Knott, G. D. (2001), 'Modeling tumor regrowth and immunotherapy', *Mathematical and Computer Modelling* **33**(12-13), 1275–1287.

Kuznetsov, V., Makalkin, I., Taylor, M. & Perelson, A. (1994), 'Nonlinear dynamics of immunogenic tumors: Parameter estimation and global bifurcation analysis', *Bull Math Biol* **56**(2), 295–321.

Lee, S. P., Leu, M. Y., Smathers, J. B., McBride, W. H., Parker, R. G. & Withers, H. R. (1995), 'Biologically effective dose distribution based on the linear quadratic model and its clinical relevance', *International Journal of Radiation Oncology Biology Physics* **33**(2), 375–389.

Leith, J. T., Padfield, G., Faulkner, L. E., Quinn, P. & Michelson, S. (1991), 'Effects of feeder cells on the x-ray sensitivity of human colon cancer cells', *Radiotherapy and Oncology* **21**(1), 53–59.

Maier, P., Hartmann, L., Wenz, F. & Herskind, C. (2016), 'Cellular pathways in response to ionizing radiation and their targetability for tumor radiosensitization', *International journal of molecular sciences* **17**(1), 102.

Moeller, B. J., Richardson, R. A. & Dewhirst, M. W. (2007), 'Hypoxia and radiotherapy: opportunities for improved outcomes in cancer treatment', *Cancer and Metastasis Reviews* **26**(2), 241–248.

Pawlik, T. M. & Keyomarsi, K. (2004), 'Role of cell cycle in mediating sensitivity to radiotherapy', *International Journal of Radiation Oncology* Biology* Physics* **59**(4), 928–942.

Prise, K. M. & O'sullivan, J. M. (2009), 'Radiation-induced bystander signalling in cancer therapy', *Nature Reviews Cancer* **9**(5), 351–360.

Reppas, A., Alfonso, J. & Hatzikirou, H. (2016), 'In silico tumor control induced via alternating immunostimulating and immunosuppressive phases', *Virulence* **7**(2), 174–186.

Rockwell, S., Dobrucki, I. T., Kim, E. Y., Marrison, S. T. & Vu, V. T. (2009), 'Hypoxia and radiation therapy: past history, ongoing research, and future promise', *Current molecular medicine* **9**(4), 442–458.

Schmitz, J. E., Kansal, A. R. & Torquato, S. (2002), 'A cellular automaton model of brain tumor treatment and resistance', *Computational and Mathematical Methods in Medicine* **4**(4), 223–239.

Schnarr, K., Dayes, I., Sathya, J. & Boreham, D. (2007), 'Individual radiosensitivity and its relevance to health physics', *Dose-Response* **5**(4), dose–response.

Stylianopoulos, T., Martin, J., Chauhan, V., Jain, S., Diop-Frimpong, B., Bardeesy, N., Smith, B., Ferrone, C., Hornicek, F., Boucher, Y., Munn, L. & R. K., J. (2012), 'Causes, consequences, and remedies for growth-induced solid stress in murine and human tumors', *Proc Natl Acad Sci U S A* **109**(38), 15101–15108.

Su, B., Zhou, W., Dorman, K. & Jones, D. (2009), 'Mathematical modelling of immune response in tissues', *Comput Math Methods Med* **10**(1), 9–38.

Vatner, R. E., Cooper, B. T., Vanpouille-Box, C., Demaria, S. & Formenti, S. C. (2014), 'Combinations of immunotherapy and radiation in cancer therapy', *Frontiers in oncology* **4**(325).

Weichselbaum, R. R., Liang, H., Deng, L. & Fu, Y.-X. (2017), 'Radiotherapy and immunotherapy: a beneficial liaison?', *Nature Reviews Clinical Oncology* **14**(6), 365–379.